

Arsenic, vanadium, iron, and manganese biogeochemistry in a deltaic wetland, southern Louisiana, USA



Katherine Telfeyan^{a,*}, Alexander Breaux^{a,b}, Jihyuk Kim^c, Jaye E. Cable^c, Alexander S. Kolker^{a,b}, Deborah A. Grimm^d, Karen H. Johannesson^a

^a Department of Earth and Environmental Sciences, Tulane University, New Orleans, LA 70118, USA

^b Louisiana Universities Marine Consortium, Cocodrie, LA 70344, USA

^c Department of Marine Sciences, University of North Carolina at Chapel Hill, Chapel Hill, NC 27514, USA

^d Coordinated Instrumentation Facility, Tulane University, New Orleans, LA 70118, USA

ARTICLE INFO

Keywords:

Vanadium
Arsenic
Subterranean estuary
Myrtle Grove
Wetland biogeochemistry
Redox-sensitive trace elements
Diffusive fluxes

ABSTRACT

Geochemical cycling of the redox-sensitive trace elements arsenic (As) and vanadium (V) was examined in shallow pore waters from a marsh in an interdistributary embayment of the lower Mississippi River Delta. In particular, we explore how redox changes with depth and distance from the Mississippi River affect As and V cycling in the marsh pore waters. Previous geophysical surveys and radon mass balance calculations suggested that Myrtle Grove Canal and the bordering marsh receive fresh groundwater, derived in large part from seepage of the Mississippi River, which subsequently mixes with brackish waters of Barataria Bay. Additionally, the redox geochemistry of pore waters in the wetlands is affected by Fe and S cycling in the shallow subsurface (0–20 cm). Sediments with high organic matter content undergo SO_4^{2-} reduction, a process ubiquitous in the shallow subsurface but largely absent at greater depths (~3 m). Instead, at depth, in the absence of organic-rich sediments, Fe concentrations are elevated, suggesting that reduction of Fe(III) oxides/oxyhydroxides buffers redox conditions. Arsenic and V cycling in the shallow subsurface are decoupled from their behavior at depth, where both V and As appear to be removed from solution by either diffusion or adsorption onto, or co-precipitation with, authigenic minerals within the deeper aquifer sediments. Pore water As concentrations are greatest in the shallow subsurface (e.g., up to 315 nmol kg^{-1} in the top ~20 cm of the sediment) but decrease with depth, reaching values $< 30 \text{ nmol kg}^{-1}$ at depths between 3 and 4 m. Vanadium concentrations appear to be tightly coupled to Fe cycling in the shallow subsurface, but at depth, V may be adsorbed to clay or sedimentary organic matter (SOM). Diffusive fluxes are calculated to examine the export of trace elements from the shallow marsh pore waters to the overlying canal water that floods the marsh. The computed fluxes suggest that the shallow sediment serves as a source of Fe, Mn, and As to the surface waters, whereas the sediments act as a sink for V. Iron and Mn fluxes are substantial, ranging from 50 to 30,000 and 770 to 4300 $\text{nmol cm}^{-2} \text{ yr}^{-1}$, respectively, whereas As fluxes are much less, ranging from 2.1 to 17 $\text{nmol cm}^{-2} \text{ yr}^{-1}$. Vanadium fluxes range from $3.0 \text{ nmol cm}^{-2} \text{ yr}^{-1}$ directed into the sediment to $1.7 \text{ nmol cm}^{-2} \text{ yr}^{-1}$ directed out of the sediment.

1. Introduction

1.1. Biogeochemistry and hydrology of coastal wetlands

The hydrology of coastal wetlands is complex and incorporates mixing of numerous hydrologic reservoirs, including surface waters and groundwaters (Fagherazzi et al., 2013; Sanders et al., 2015). Additionally, chemical constituents (e.g., carbon, nutrients, metals) of shallow and deep pore waters flowing through wetlands may be substantially different than those of the surface estuary owing to input from

terrestrial aquifers, adsorption/desorption reactions with mineral surfaces within the sediments, and biogeochemical reactions that occur where groundwater with enriched reduced species (e.g., Fe^{2+} , Mn^{2+} , HS^- , etc.) encounters oxygenated marine waters (Moore, 1999; Gleeson et al., 2013; Maher et al., 2013; Sanders et al., 2015; Makings et al., 2014). The difference in concentrations of solutes in pore water and overlying water in such environments leads to a chemically reactive zone, termed the subterranean estuary (STE) where fresh and saline water mix within sediments in coastal aquifers (Moore, 1999).

* Corresponding author at: Earth and Environmental Sciences Division, Los Alamos National Laboratory, Los Alamos, NM 87545, USA.
E-mail address: ktelfeya@tulane.edu (K. Telfeyan).

Biogeochemical reactions occurring in the STE may immobilize solutes within, or release solutes from, sediments into pore water, thus potentially altering the flux of solutes to the ocean (Berner, 1980; Moore, 1999; Cable et al., 1996; Charette and Sholkovitz, 2006; Santos et al., 2011). For example, water discharged from the STE may act as a source of nutrients (Slomp and Van Cappellen, 2004; Paytan et al., 2006), silica (Kim et al., 2005), carbon (Cai et al., 2003; Moore et al., 2006), and iron (Windom et al., 2006; Charette et al., 2007) and may also affect the mass balance of oceanic tracers, such as Nd and its isotopes (Johannesson and Burdige, 2007; Johannesson et al., 2011; Chevris et al., 2015a) or Sr (Basu et al., 2001; Charette and Sholkovitz, 2006) to the coastal ocean. Moreover, studies of a number of redox-sensitive trace elements (e.g., Mo, U, V, Fe, Hg, As) demonstrate that the STE can serve as a source or sink of these trace elements depending on the geologic setting and dominant biogeochemical reactions occurring in the STE (e.g., Windom and Niencheski, 2003; Bone et al., 2006; Swarzenski and Baskaran, 2007; Gonneea et al., 2014; O'Connor et al., 2015). For example, the STE may serve as a sink for uranium when oxidized marine water recirculates through reducing sediments (O'Connor et al., 2015), or as a source of uranium when coastal aquifer materials are enriched in uranium (e.g., phosphatic desposits; Swarzenski and Baskaran, 2007). Many of these redox-sensitive trace elements (e.g., Mo, U, Re, V) are important as paleo-redox tracers of past ocean chemistry, and hence, understanding the coastal processes that control their fluxes and cycling is essential for interpreting chemical signatures in ancient marine rocks (e.g., Trefry and Metz, 1989; Rimmer, 2004; Morford et al., 2005; Tribovillard et al., 2006).

Flow of pore water through the STE of coastal wetlands is further complicated by Fe, S, and organic matter cycling within the marsh environment (Stump et al., 2014). Whereas burial of carbon is important in Louisiana marshes, where deposition rates can reach 1 cm yr^{-1} in environments like those discussed in this paper (DeLaune et al., 2003; Kirman et al., 2016), much of the primary productivity in a marsh is subjected to either remineralization or erosion from the marsh to the coast (Fagherazzi et al., 2013). Marshes in many Louisiana estuaries are net erosional (Couvillion et al., 2011; Wilson and Allison, 2008), with organic material both recycled in the estuary and exported to the coast (Bianchi et al., 2011a). In salt marshes, the majority of the organic matter remineralization occurs in the top 20 cm of the sediment where the system is sensitive to changes in tides, rainfall, temperature, and vegetation growth (Lord and Church, 1983; Hunt et al., 1997; Báez-Cazull et al., 2008). Organic matter remineralization in sediments occurs during anaerobic respiration whereby microbes utilize oxidants for energy in order to conserve the most energy per mole of organic carbon consumed such that the energetic favorability of the oxidants (electron acceptors) decreases as follows: $\text{O}_2 > \text{Mn}^{(\text{IV})}\text{O}_2 \sim \text{NO}_3^- > \text{Fe}^{(\text{III})}\text{O}_2 > \text{SO}_4^{2-}$ (Froelich et al., 1979). However, the specific electron acceptor used by microbes to oxidize organic matter during anaerobic respiration, as well as the depth of reduction, varies as a function of the sediment organic matter content, diffusive flux of oxygen, physical heterogeneity in the subsurface from roots, bioturbation by benthic animals, and the supply of possible oxidants (Aller, 1982; Craven et al., 1986; Gaillard et al., 1989; Shaw et al., 1990; Burdige, 1993). In salt marshes, sulfate reduction is commonly responsible for as much as 90% of the organic matter remineralization, with iron and manganese reduction playing relatively minor roles when compared to sulfate reduction (Gaillard et al., 1989; Burdige, 1993; Carey and Taillefert, 2005).

1.2. Arsenic and vanadium geochemistry

Arsenic is a highly toxic element, with increasing toxicity from organic As to inorganic arsenate and inorganic arsenite (B'hymer and Caruso, 2004). Arsenate is chemically similar to phosphate and therefore is a competitive inhibitor, leading to uptake of arsenate by

phytoplankton in P-limited waters (Hellweger et al., 2003; Duan et al., 2010; Ren et al., 2010). Similarly, although V is essential to biota at low concentrations, at higher concentrations V(V) impedes the functionality of Na^+/K^+ -dependent ATPase, and consequently, can be detrimental to organisms (Cantley and Aisen, 1979). Arsenic in natural waters exists predominantly in the As(III) and As(V) redox states, occurring as oxyanions, oxythioanions, or in organic compounds such as methylated species and organosugars (Cullen and Reimer, 1989; Webster, 1990; Planer-Friedrich et al., 2007; Helz and Tossell, 2008). Arsenic in groundwater systems has been studied extensively in conjunction with Fe and Mn cycling owing to the prevalence of As contamination in Holocene deltaic aquifers undergoing reductive dissolution of Fe(III)/Mn(IV)oxides/oxyhydroxides (e.g., Nickson et al., 1998; Fendorf et al., 2010; Yang et al., 2016). However, in systems with elevated dissolved sulfide, formation of thioarsenates will also influence arsenic cycling (Hollibaugh et al., 2005; Wallschläger and Stadey, 2007; Planer-Friedrich et al., 2008). Thus, further study of arsenic in sulfidic wetland environments is warranted.

Vanadium is a lithophilic element that predominantly exists in natural waters as oxyanions of V(V) and oxycations of V(IV), although V(III) can exist in extremely reducing environments (Goldschmidt, 1954; Wanty and Goldhaber, 1992). Whereas the vanadate oxyanion $\text{H}_2\text{V}^{(\text{V})}\text{O}_4^-$ is stable in solution in oxidized waters, the vanadyl cation, $\text{V}^{(\text{IV})}\text{O}^{2+}$, which predominates in many reducing waters, is particle reactive and commonly adsorbs to clays and organic matter (McBride, 1979; Breit and Wanty, 1991; Wanty and Goldhaber, 1992). Vanadium geochemistry has also been explored in terrestrial aquifers (Fiorentino et al., 2007; Wright and Belitz, 2010; Pourret et al., 2012; Wright et al., 2014) as well as in the ocean (Jeandel et al., 1987; Middelburg et al., 1988), but studies of its cycling in the coastal zone are fewer (Beck et al., 2008; Beck et al., 2010; O'Connor et al., 2015).

The hydrologic and geochemical dynamics of salt marsh systems are known to exert important controls on trace metal cycling in shallow pore waters, which may change diurnally or seasonally and be largely decoupled from deeper pore waters (Beck et al., 2008). In this contribution, we focus on As and V cycling because of their redox sensitivity, potential role as environmental contaminants, and importance in biological cycles. We use the current understanding of V and As redox-sensitivity and speciation controls to investigate their cycling in a coastal wetland where groundwater predominantly sourced from the Mississippi River mixes with brackish water from Barataria Bay (Kim, 2015). We examine how As and V concentrations vary within the context of marsh hydrology and predominant redox processes. Although we focus on a marsh in the Mississippi River Delta, the implications of this study shed light on the complexities of trace element cycling in wetlands of other major river delta systems.

2. Study site

The Myrtle Grove study site is located in the Barataria Basin, an intertributary basin within the larger Mississippi River Delta that is constrained by the Mississippi River to the east, Bayou Lafourche to the west, and the Gulf of Mexico to the south (Fig. 1; Breaux, 2015; Kim, 2015). Barataria Basin encompasses a region of about 6300 km² (Park, 2002; Inoue et al., 2008). Myrtle Grove Canal (MG) is a ~20 km long north-south oriented canal in the southern portion of Barataria Basin extending from ~1 km south of the Mississippi River to the head of Barataria Bay (Fig. 1). Surface water salinities range from ~4 in the northern portion of the canal proximal to the Mississippi River to ~8 closer to the Bay (Table 1). With the gradual increase in salinity from north to south along the canal, the vegetation also changes from predominantly *Spartina patens* and *Distichlis spicata* at the head of the canal in the brackish marsh to *Spartina alterniflora* and *Juncus roemerianus* closest to the Bay in the salt marsh (CRMS, 2015; lacoast.gov/crms). The sediment throughout the marsh is similar to other brackish-salt marsh systems, consisting of predominantly porous organic matter

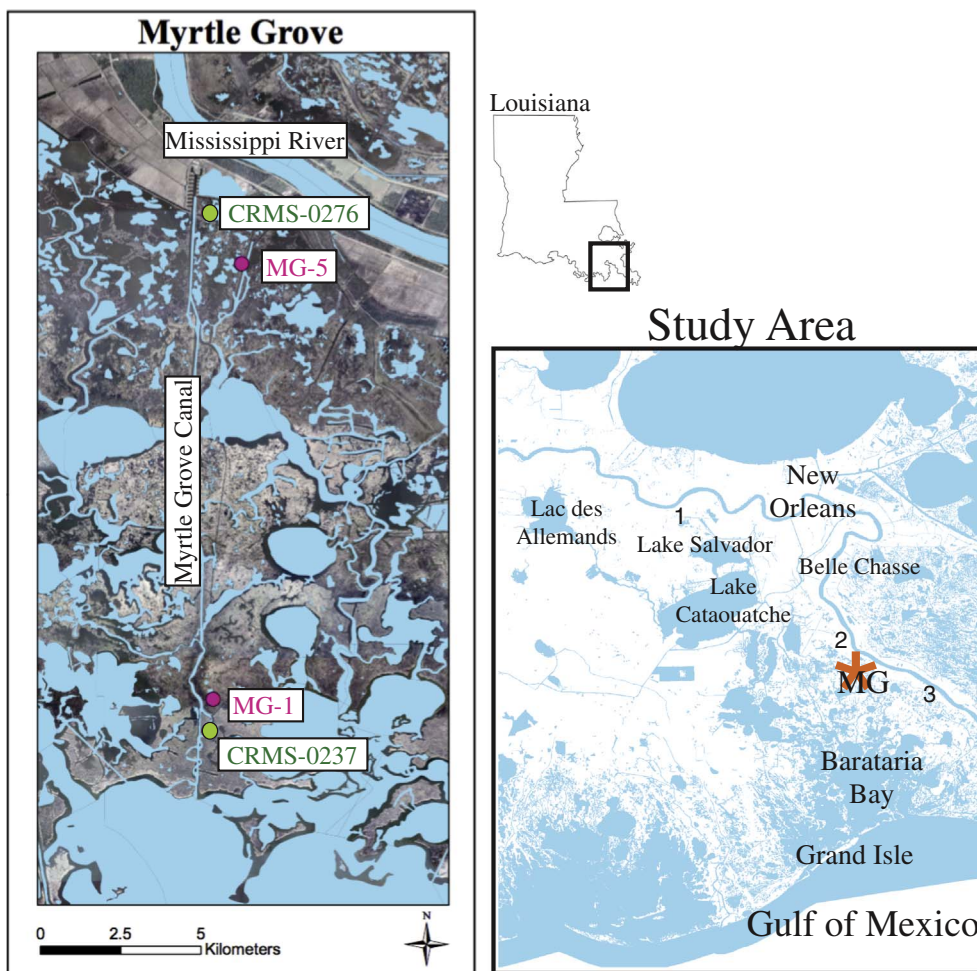


Fig. 1. Map of sample sites along Myrtle Grove Canal. At MG-1 and MG-5, samples were collected from surface water in the canal adjacent to the piezometers installed nearby. The short sediment cores were collected within 200 m of the piezometers. Coastwide Reference Monitoring System stations CRMS0276 and CRMS0237 are also shown (green). Freshwater diversions are indicated as (1) Davis Pond Diversion, (2) Naomi Siphon, and (3) West Point à la Hache Siphon. (For interpretation of the references to colour in this figure legend, the reader is referred to the web version of this article.)

in the top ~50 cm that becomes chiefly sandy or silty loams with depth (Hughes et al., 1998; Breaux, 2015; O'Connor and Moffett, 2015). The tides at Barataria Pass are diurnal, typical of the Gulf of Mexico, and reach a maximum tidal range of ~0.6 m. Flushing times of Barataria Bay are estimated to be 13–19 days (Li et al., 2011). The greatest water level fluctuations and hydrological exchanges occur during the passages of cold fronts, which occur on a ~weekly basis from October to April (Li et al., 2011).

Barataria Basin receives freshwater from rainfall, artificial river diversions, the Gulf Intracoastal Waterway, and surface runoff (Das et al., 2010; Bianchi et al., 2011b). Additionally, groundwater may be supplied to Barataria Basin through buried paleochannels driven by differences in hydraulic head between the Mississippi River and marshes (Kolker et al., 2013; Breaux, 2015; Kim, 2015).

Land loss in this part of the delta is substantial owing to a combination of subsidence, sea level rise, dredging, flood control levees, and movement on listric normal faults (Couvillion et al., 2011; Day et al., 2007; Kolker et al., 2011; Shen et al., 2016). As such, anthropogenic freshwater diversions from the Mississippi River have been constructed to supplement rainfall and the Gulf Intracoastal Waterway as freshwater sources to the basin and deliver sediment to the subsiding wetlands (Fig. 1; Das et al., 2010, 2012). As part of the Louisiana's Comprehensive Master Plan for a Sustainable Coast, the Mid Barataria Diversion proposed for Myrtle Grove would discharge $2124 \text{ m}^3 \text{ s}^{-1}$ of Mississippi River water to the Myrtle Grove Canal (Das et al., 2012; LACPR, 2012, <http://coastal.la.gov/2017-coastal->

[master-plan](#)). Consequently, understanding the hydrology and geochemistry of the Myrtle Grove region is critical to predicting the utility and effect of any potential future river diversion in the area.

The two sample sites, MG-5 and MG-1, differ in their proximity to the Mississippi River and vegetation type (Fig. 1). Site MG-5 is located ~2.75 km from the Mississippi River (~1.75 km from the head of MG), and the short core taken for pore water extraction (Section 3.3) at this site was collected from a tidal flat that was separated from Myrtle Grove Canal by ~50 m of a brackish marsh (salinity ~4). During the April 2014 sampling the tidal flat was exposed to the atmosphere, whereas during the September 2014 sampling, the tidal flat was flooded with water. As a consequence of the marsh flooding, the short core was collected from an exposed portion of the tidal flat bank. MG-1, which is ~15 km from the Mississippi River, is vegetated by *Spartina alterniflora*, which is indicative of the greater salinity (up to 9) of the marsh at this location (Fig. 1).

3. Methods

3.1. Hydrological measurements

We compiled hydrologic data from the United States Geological Survey (USGS), National Oceanic and Atmospheric Administration (NOAA), Coastwide Reference Monitoring System (CRMS), and our own monitoring stations to evaluate the important variables affecting water level and salinity within the marsh (waterdata.usgs.gov; tide-

Table 1
Concentrations of measured parameters for surface waters (SW), shallow pore waters (PW), and groundwaters (GW) for sites MG-1 and MG-5 sampled in April and September 2014.

Sample	Depth (cm)	Salinity	pH	S(−II) ^a ($\mu\text{mol kg}^{-1}$)	SO ₄ ^{2−b} (mmol kg^{-1})	Fe ($\mu\text{mol kg}^{-1}$)	Mn ($\mu\text{mol kg}^{-1}$)	V (nmol kg^{-1})	As nmol kg^{-1})
April 10–13, 2014									
MG-1-SW	Canal surface water	6.29	6.39	3.6	3.3	0.1	0.9 ± 0.1	19.6	12.5 ± 0.1
MG-1-PW1	0–1.5		7.15	84.8		0.6	8.2	30.7 ± 2.1	125.5 ± 5.3
MG-1-PW2	1.5–3.0			356.7		1.1	9.0 ± 0.2	35.2 ± 0.5	142.7 ± 7.3
MG-1-PW3	3.0–5.5			117.3		5.0	7.7	36.8 ± 0.4	216.2 ± 2.3
MG-1-PW4	5.5–8.2			457.2		1.5	9.4 ± 0.2	26.3 ± 0.5	222.7 ± 8.5
MG-1-PW5	8.2–9.7		7.50	198.6		0.4	8.8 ± 0.2	23.8 ± 0.7	212.5 ± 10.7
MG-1-PW6	9.7–12.0		7.47	283.4		0.4	9.6	20.7 ± 0.2	315.4 ± 3.7
MG-1-PW7	12.0–16.0		7.53	292.4		1.6	9.9 ± 0.1	20.0 ± 0.6	302.3 ± 8.6
MG-1-GW	357	22.0	5.75	1.6	2.2	37.0 ± 0.3	33.8 ± 0.2	31.2	10.3
MG-5-SW	Canal surface water	4.05	8.49	1.1	1.9	0.5	0.6	25.0	12.2
MG-5-PW1	0–2.0		7.20	2.8		5.9 ± 0.1	14.7 ± 0.4	14.1 ± 0.3	34.4 ± 0.8
MG-5-PW2	2.0–3.1		7.19	6.2		2.1	12.4 ± 0.1	12.0	23.8 ± 1.4
MG-5-PW3	3.1–4.7		7.31	17.2		0.8	12.6 ± 0.1	13.3 ± 0.7	21.3 ± 0.6
MG-5-PW4	4.7–6.3		7.64	9.4		1.4	12.8 ± 0.2	13.4 ± 0.8	59.1 ± 2.2
MG-5-PW5	6.3–7.6			34.9		0.9	10.3	13.8 ± 0.8	30.8 ± 1.0
MG-5-PW6	7.6–9.1		7.60	69.5		6.4 ± 0.1	10.0	34.4 ± 0.4	32.8 ± 0.7
MG-5-PW7	9.1–11.0		7.64	57.1		1.9	8.0 ± 0.1	14.5 ± 0.2	24.3 ± 0.4
MG-5-PW8	11.0–13.1		7.47	37.4		0.5	6.81 ± 0.11	10.3 ± 0.4	22.8
MG-5-PW9	13.1–15.0			44.0		1.1	7.16 ± 0.1	11.1 ± 0.2	40.4 ± 0.7
MG-5-GW	302	0.811	7.01	0.8	BDL ^c	44.0 ± 0.2	14.1	41.4	27.8
September 23, 2014									
MG-1-SW	Canal surface water	9.91	7.89	1.4	2.92	0.7 ± 0.1	0.6	37.8 ± 0.5	15.8 ± 0.5
MG-1-PW1	0–2.3	5.00	6.26	0.7		393.4 ± 5.3	58.9 ± 0.6	23.9 ± 0.5	94.3 ± 1.7
MG-1-PW2	2.3–3.6		6.55	5.5		545.5 ± 9.8	67.6 ± 1.1		126.1 ± 3.96
MG-1-PW3	3.6–5.2		6.79	8.8		489.5 ± 15.0	64.9 ± 1.8	51.8 ± 1.0	122.6 ± 7.6
MG-1-PW4	5.2–6.9		6.60	3.2		803.8 ± 33.7	83.0 ± 2.7	71.6 ± 2.8	210.6 ± 4.1
MG-1-PW5	6.9–8.2			6.6		637.8 ± 23.6	77.1 ± 1.4	73.3 ± 2.2	201.3 ± 18.4
MG-1-PW6	8.2–9.3	6.00				444.4 ± 11.4	53.5 ± 1.0	36.0 ± 0.6	142.0 ± 12.5
MG-1-PW7	9.3–12.5		6.57			572.7 ± 38.0	59.5 ± 2.6	39.2 ± 2.0	164.8 ± 4.8
MG-1-GW	357	10.4	6.78	BDL ^c	2.8	307.2 ± 12.1	56.8 ± 1.6	7.1	2.4 ± 0.2
MG-5-SW	Canal surface water	4.53	8.17	0.8	0.5	0.1	4.5	59.8 ± 0.7	28.3 ± 1.0
MG-5-PW1	0–1.6	5.00	6.48	782.4		6.9 ± 0.1	21.4 ± 0.2	36.6 ± 0.6	51.1 ± 3.2
MG-5-PW2	1.6–3.2		6.46	661.2		2.5 ± 0.1	16.9 ± 0.3	26.7 ± 1.6	37.0 ± 3.0
MG-5-PW3	3.2–4.3		6.58	344.9		2.4 ± 0.1	14.6 ± 0.9	31.0 ± 0.5	25.8 ± 0.9
MG-5-PW4	4.3–5.8		6.65	785.9		0.9	14.5 ± 0.4	28.9 ± 0.8	31.1 ± 0.6
MG-5-PW5	5.8–7.1		6.64	355.5		1.5	11.9 ± 0.2	36.2 ± 0.5	23.0 ± 0.8
MG-5-PW6	7.1–8.8	6.00	6.69	580.0		5.1 ± 0.5	12.7 ± 0.7	54.5 ± 3.1	27.6 ± 1.8
MG-5-PW7	8.8–10.5		6.87	620.6			10.8 ± 0.1	27.9 ± 0.1	23.8 ± 0.6
MG-5-PW8	10.5–13.6	5.00	6.80	888.8		0.5	10.4	29.3 ± 0.7	21.3 ± 0.7
MG-5-GW	302	3.57	7.15	2.7	2.6	68.0 ± 0.3	10.6 ± 0.5	46.5 ± 0.2	8.0 ± 0.2

^a Accuracy of the spectrophotometric method is 10% (APHA, 1985).

^b Relative standard deviation of the spectrophotometric method is 1.7% (APHA, 1985).

^c Sample below detection limit.

sandcurrents.noaa.gov; lacoast.gov/crms). The CRMS maintains two stations proximal to our study site that record the marsh water level on a daily basis (Fig. 1; CRMS-0276, CRMS-0237). A NOAA tidal station provided hourly tidal level at Grand Isle, a barrier island located at the southern boundary of Barataria Bay (Fig. 1). The river stage was reported daily from a gauging station at Belle Chasse maintained by the USGS. Additionally, CTD divers were installed in our piezometers (see Section 3.2. below) to record hourly water level and temperature for the period between May 27 and September 24, 2014. A fast Fourier transform function was used in Matlab (vR2015b) to convert these time series data to frequency in order to identify the most dominant periods in the hydrologic data (Menke and Menke, 2012; O'Connor and Moffett, 2015).

3.2. Sampling

Piezometers at sites MG-1 and MG-5 at Myrtle Grove were installed to depths of ~3–4 m in the marsh on the eastern edge of the Myrtle Grove Canal in April 2014 after extraction of sediment cores from the same locations (Fig. 1). Sediment cores were extracted using vibracoring techniques and were processed for grain size analysis and loss on ignition (Breau, 2015). Immediately after core withdrawal, the piezo-

meters were emplaced and packed with sand (Quikrete® All-Purpose Sand). Piezometers were constructed from PVC pipes connected to a PVC Well Point that contained a 0.91 m screened interval. Prior to sample collection, piezometers were developed by pumping to dryness. Hereafter, we will refer to water collected from the piezometers as groundwaters to differentiate between the shallow pore waters extracted from the shallow sediment cores that are described below.

Piezometer and surface water sampling surveys at Myrtle Grove Canal were conducted during April and September 2014. Sampling equipment, including high-density polyethylene (HDPE) sample bottles and Teflon® tubing, were rigorously cleaned prior to use following trace-metal clean procedures as described previously (e.g., Johannesson et al., 2004). Pore waters were pumped from each piezometer using a peristaltic pump with Teflon® tubing attached to a 0.45- μm Gelman Sciences (polysulfone ether membrane) in-line filter capsule after rinsing the HDPE sample bottle three times with the filtered sample water. Surface water samples were similarly collected from just below the water surface of the canal proximal to each piezometer. All filtered water samples were then acidified so that the final sample volume consisted of 1% (v/v) ultrapure HNO₃ (15.8 M, Thermo Fisher Optima™) and had a pH < 2. Deionized water was taken into the field and processed as a sample (i.e., field blank) to ensure no contamination

during the sampling process, and duplicate samples were collected in the field to quantify analytical precision. Samples were kept in a cooler on ice in the field and transferred to a refrigerator ($\sim 4^\circ\text{C}$) at Tulane University where they were stored until analysis. Trace element analysis of the water samples was conducted within two weeks of sample collection.

Ancillary geochemical parameters, including salinity and pH were determined on-site using a YSI handheld multiparameter sonde and Oakton[®] pH meter (calibrated daily), respectively. Dissolved S(-II) and SO_4^{2-} were determined using a portable Hach DR 2800 UV-VIS spectrophotometer. Dissolved S(-II) concentrations were measured using the methylene blue method (detection limit $0.31\ \mu\text{mol kg}^{-1}$; Eaton et al., 1995), and SO_4^{2-} concentrations were determined by the SulfaVer[®] method (detection limit $0.02\ \text{mmol kg}^{-1}$; Eaton, 2005).

3.3. Core collection and processing

Shallow pore waters were extracted from shallow sediment cores (10–20 cm) that were collected in April and September of 2014. The cores were rich in organic matter and core MG-1 contained plant materials (mostly roots) (Breux, 2015). A Hargis corer was used to extract the sediment cores, which were immediately transferred to an acid-rinsed (3.2 M HNO_3) acrylic tube (2 mm thick walls, 6.8 cm inner diameter). The samples were immediately capped, taped, and placed in O_2 -impermeable Remel[®] anaerobic bags (Mitsubishi Gas Chemical Co., Remel[®]; Cat. No. 2019-11-02). Addition of an O_2 absorber pouch (Mitsubishi Gas Chemical Co., AnaeroPouch[®] Anaero; Cat. No. 23-246-379; Sankar et al., 2014) prevented oxidation of sediments and pore waters. Samples were then transported back to Tulane University and processed in a glove box under a nitrogen atmosphere the same day.

The sediment cores were sectioned in the glove box into ~ 20 mm segments measured along the core length, and the segments were then transferred into acid-washed 50 mL polyethylene centrifuge tubes (Mohajerin et al., 2016). Pore water was then extracted by centrifugation (20 min at a relative centrifugal force of 1996) under N_2 . The resultant pore water was then partitioned in the glove box as follows. Approximately 1 mL of sample was diluted to 10 mL total volume with deoxygenated, doubly distilled (Milli-Q, $18\ \text{M}\Omega\ \text{cm}$) water and transferred outside the glove box for immediate UV-VIS spectrophotometry analysis (Hach DR 5000) of S(-II) by the methylene blue method as mentioned above. Another aliquot (approximately 2 mL) was filtered in the glove box through $0.45\ \mu\text{m}$ Gelman PTFE filters into a 15 mL polyethylene test tube. The filtered pore waters were then transferred to a class 100, laminar flow clean bench where they were diluted with approximately 8 mL of 0.32 M HNO_3 (Thermo Fisher Optima[™]) and then refrigerated until analysis for trace elements. If there was sufficient pore water remaining, pH and salinity were measured using an Oakton[®] pH meter and a refractometer, respectively.

3.4. Trace metal analysis

The concentrations of trace elements were determined by sector-field inductively coupled plasma mass spectrometry (Thermo Fisher Element 2 ICP-MS) at Tulane University. Vanadium, Mn, and Fe concentrations were determined by monitoring ^{51}V , ^{55}Mn , and ^{56}Fe , respectively, under medium resolution and As was measured by monitoring ^{75}As under high resolution to distinguish it from potential ArCl^+ interferences in the plasma stream (Datta et al., 2011; Olesik, 2014; Yang et al., 2015). A ^{45}Sc spike ($222.4\ \text{nmol kg}^{-1}$) was monitored as the internal standard for both medium and high resolution runs. Calibration standards were made in concentrations ranging from $5\ \text{ng kg}^{-1}$ to $2.5\ \text{mg kg}^{-1}$ from SPEX CertiPrep[®] ICP-MS Multi-Element Solution 2 with 0.32 M HNO_3 . The accuracy of each analysis was evaluated using check standards in addition to the National Institute of Standards and Technology (NIST) Standard Reference Material 1643e

(Trace Elements in Water), the National Research Council of Canada (NRCC) SLEW-3 (Estuarine Water), and NRCC SLRS-4 (River Water Reference Material). Percent error was generally $< 10\%$.

3.5. Geochemical modeling

Geochemical modeling of dissolved species and mineral saturation states was performed using the SpecE8 and React programs of Geochemist's Workbench[®] (version 9.0; Bethke, 2008). The entire suite of elements used in the geochemical calculations is listed in Appendix A. Thermodynamic data from the default database (i.e., thermo.dat) constructed by the Lawrence Livermore National Laboratory Database (Delany and Lundeen, 1990) was modified to include the dissociation constants of arsenous and arsenic acids from Nordstrom et al. (2014), the sulfidation reactions for As from Helz and Tossell (2008), and solubility data for Fe- and As-sulfide minerals from Morse et al. (1987), Webster (1990), Eary (1992), Nordstrom and Archer (2003), Rickard (2006), and Nordstrom et al. (2014), as outlined in Yang et al. (2015). To date, the most appropriate formation constants of thioarsenates are those reported in Helz and Tossell (2008), which were estimated by ab initio computations. Arsenic speciation prediction using these constants is deficient because the model assumes that all As(III) is able to form thioarsenite and As(V) to form thioarsenate, but without quantification of zero-valent sulfur in the shallow porewaters, the speciation of As cannot be decisively quantified (Jay et al., 2004; Helz, 2014). Nevertheless, the thioarsenic speciation model is thought to be accurate within roughly a factor of 10 of the actual species distributions (Helz and Tossell, 2008; Yang et al., 2015).

3.6. Flux calculations

In order to determine the transport of trace elements between hydrologic reservoirs, we consider the one dimensional transport equation that accounts for advection, bioturbation, and diffusion (Smith et al., 2008; Chevis et al., 2015b). We did not observe active bioturbation by benthic animals within Myrtle Grove sediments, and although roots are present throughout the marsh, their effect is to increase porosity, which is accounted for in the diffusion equation. Additionally, Kim (2015) used Rn measurements to investigate advection between marsh sediments and canal water, which was deemed to be negligible. Therefore, the advective-dispersive equation simplifies to the diffusion equation. Diffusive fluxes of trace elements from shallow Myrtle Grove pore waters were therefore calculated using Fick's first law of diffusion:

$$J_{diff} = -\phi D_s \frac{\partial C}{\partial z} \quad (1)$$

in which ϕ is the porosity, D_s is the bulk sedimentary diffusion coefficient ($\text{m}^2\ \text{sec}^{-1}$), and $\partial C/\partial z$ is the concentration gradient, which is approximated by $\Delta C/\Delta z$ (Berner, 1980; Burdige, 2006) (Table 2). Depth is positive in the downward direction. Thus, the negative sign

Table 2
Constants used in Eq. (1).

Constant	Value	Source
ϕ	0.89 ± 0.03	Breux (2015)
$D_{sw}\ (\text{m}^2/\text{s})$	As: $9.05\ 10^{-10}$ Fe: $7.19\ 10^{-10}$ Mn: $6.88\ 10^{-10}$ V: $7.93\ 10^{-10}$ (vanadyl), $8.46\ 10^{-10}$ (vanadate)	Li and Gregory (1974)

To the best of our knowledge, there is no value reported for V. Additionally, using the Stokes-Einstein equation to derive a coefficient is not suitable for the oxyanion species. Therefore, we used the value for ions with similar charge and molecular weight. Vanadyl is most similar to the Ca^{++} ion, whereas vanadate is most similar to the H_2PO_4^- ion.

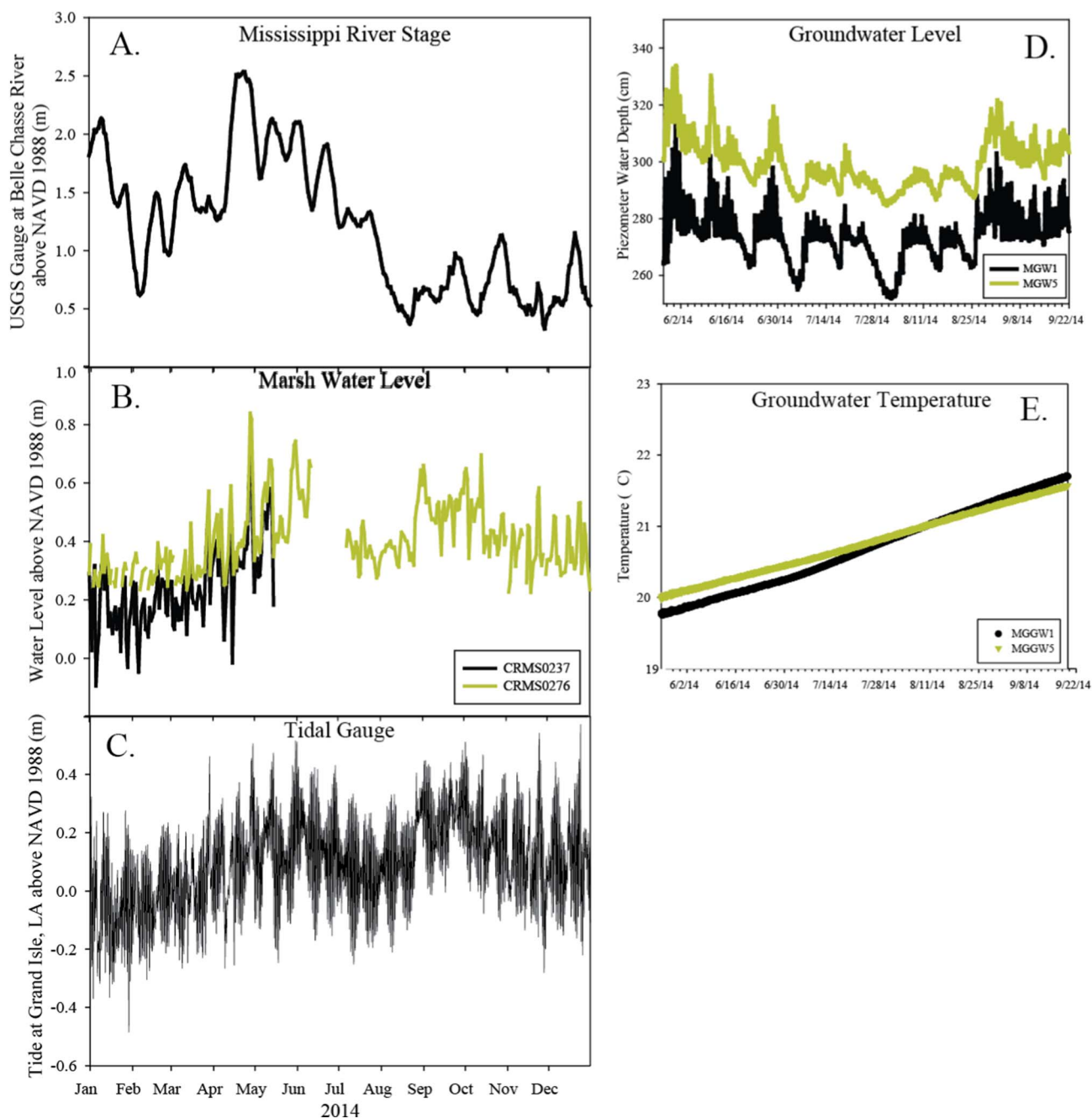


Fig. 2. A. Time series data for the Mississippi River stage measured at Belle Chasse (A), the surface water level in the marsh reported by CRMS (B) and the NOAA tidal level measured at Grand Isle (C) for 2014 as outlined in the text. Water depth (D) and temperature (E) as recorded from CTD divers are shown for both piezometers. Sample sites MG-5 and CRMS site 0276 are located proximal to the river, whereas MG-1 and CRMS site 0237 are near Barataria Bay.

indicates that flux is negative in the upward direction. The diffusion equation accounts for tortuosity by dividing the molecular diffusion coefficient by the tortuosity factor, such that, $D_s = \frac{D_{sw}}{\theta^2}$, where D_{sw} is the molecular diffusion coefficient for each element, and θ^2 is the tortuosity factor, which is calculated from $\theta = 1 - \ln(\varphi^2)$ (Table 2; Li and Gregory, 1974; Burdige, 2006).

4. Results

4.1. Marsh hydrology

Hydrologic data from lower Barataria Basin are shown in Fig. 2 as a function of time. The Mississippi River stage was greatest in the spring and lowest in the autumn and early winter (Fig. 2A). Over the course of

2014, the highest tides occurred in the late spring, decreased over the summer, and increased again in the autumn (Fig. 2C). A similar pattern is observed for the marsh water levels measured at both CRMS stations (Fig. 2B). Linear regression of the time series data indicate that water levels in the surficial marsh correlate significantly with the daily high tide level at Grand Isle (CRMS-0276, $R^2 = 0.51$, $p < 0.005$; CRMS-0237, $R^2 = 0.54$, $p < 0.005$). In contrast, water levels in piezometers MG-1 and MG-5 are only weakly positively related to the tidal fluctuations (Fig. 2D; MG-1, $R^2 = 0.25$, $p < 0.005$; MG-5, $R^2 = 0.11$, $p < 0.005$). The temperature in the deep pore waters increases over the observation period, from May 27 to September 24, 2014 (Fig. 2E).

Fourier analysis of the pressure head time series data indicates that the predominant period in pore water level is ~ 14 days, or half a lunar cycle. The daily tidal variability (24 h period) is apparent at MG-1,

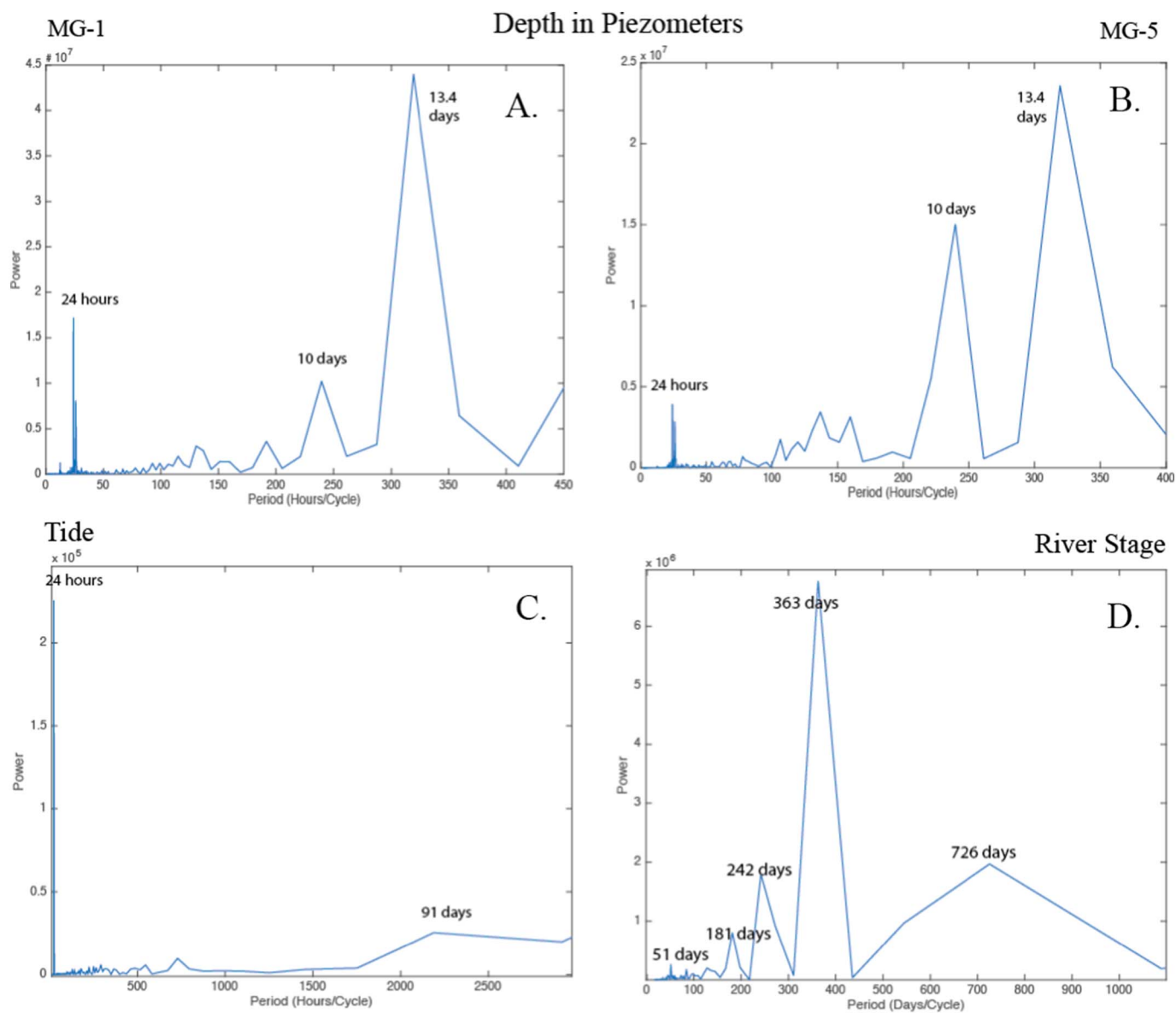


Fig. 3. Fourier transforms of the time series data from Fig. 2 displayed as recurrence periods. The variables considered are the water depths in piezometers MG-1 (A) and MG-5 (B), the water level recorded at the NOAA Grand Isle tidal gauge (C), and the Mississippi River stage recorded at the USGS Belle Chasse gauging station (D). Note that the y-axis on (A) and (B) are 10^7 , for panel (C) is 10^5 and for panel (D) is 10^6 .

which is closest to Barataria Bay but is substantially muted at MG-5, which is proximal to the river (Fig. 3A, B, C). The dominant period for the river stage is approximately 1 year (Fig. 3D).

4.2. Pore water profiles

The trace element (i.e., Fe, Mn, As, and V) and dissolved S(–II) concentrations of the surface waters, shallow pore waters, and deep groundwaters for sites MG-1 and MG-5 are presented in Figs. 4 and 5, respectively, along with porosity and loss on ignition (LOI) data from Breaux (2015). We assume that the surface waters collected from Myrtle Grove Canal are representative of the water flooding the marsh. Again, the shallow pore waters were extracted from the organic-rich, “spongy” sediments in the upper marsh, whereas the deeper groundwaters are from the mineral-rich sediments between 3 and 4 m depth below the surface. The porosity of the upper core is substantial (e.g., up to ~80%, Figs. 4, 5; Breaux, 2015), which likely reflects organic matter remineralization and/or dissection from plant roots.

4.3. General redox structure of shallow pore waters and deeper groundwaters

Dissolved sulfide concentrations are commonly greater in the shallow pore waters than in the deeper groundwaters (Table 1; Figs. 4, 5). More specifically, the shallow pore water dissolved S(–II) concentrations are 1–3 orders of magnitude greater than in the deeper groundwaters. The pore water S(–II) profiles from the MG-1 and MG-5 sites display multiple peaks in each core and exhibit seasonal differences (Figs. 4, 5). For example, in shallow pore waters from the MG-1 site, S(–II) concentrations are close to 2 orders of magnitude higher in April than September (average $256 \mu\text{mol kg}^{-1}$ vs. $4.95 \mu\text{mol kg}^{-1}$), whereas at the MG-5 site, S(–II) concentrations of the shallow pore waters are greater in September than in April (average $627 \mu\text{mol kg}^{-1}$ vs. $30.9 \mu\text{mol kg}^{-1}$).

The total dissolved Fe (passed through $< 0.45 \mu\text{m}$ pore-size filters) concentrations of the surface waters are $< 1 \mu\text{mol kg}^{-1}$ for both seasons at both locations (Table 1). At the MG-1 site near Barataria Bay, the Fe concentrations are much greater in September than in April,

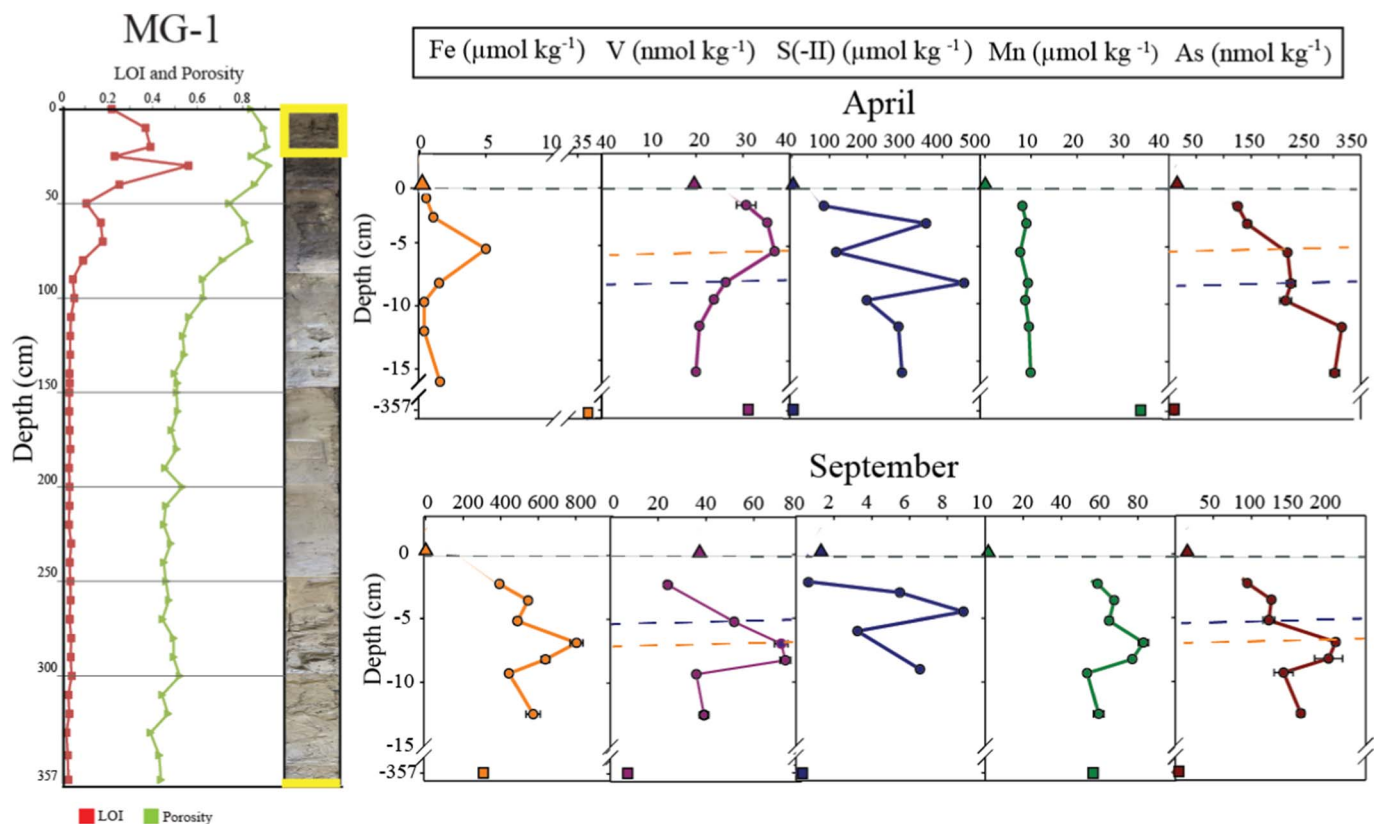


Fig. 4. Graphical summary of data presented in Table 1 for site MG-1 near Barataria Bay. The left half of the figure depicts the core image, loss on ignition (LOI) and porosity from Breaux (2015) for the length of the sediment core taken prior to piezometer emplacement. Dissolved S(-II) and trace element Fe, V, Mn, and As concentrations are shown for the surface waters in April and September (triangles), the shallow pore waters (circles), and the deeper groundwaters (squares). The grey dashed line indicates the sediment-water interface and the orange and blue dashed lines represent dissolved Fe and S(-II) peaks, respectively. The yellow outlines on the core image indicate where pore water was extracted. (For interpretation of the references to colour in this figure legend, the reader is referred to the web version of this article.)

whereas at the MG-5 site near the Mississippi River, the shallow pore water Fe concentrations exhibit less seasonal variation. Both sites exhibit elevated Fe concentrations in the deep groundwaters as compared to the shallow pore waters and surface waters. Total dissolved Mn exhibits different concentration trends than Fe in surface, shallow, and deep groundwaters (Figs. 4, 5). For example, Mn concentrations in shallow pore waters from the MG-1 site near Barataria Bay show distinct peaks with depth, whereas the Mn concentrations generally decrease with depth during April and September at the MG-5 location (Figs. 4, 5). Unlike the Fe concentrations, Mn concentrations in the deeper pore waters are comparable to those of the shallow pore waters.

The Fe and Mn concentrations of the surface waters are similar to those of the Mississippi River (Fe: $0.12 \mu\text{mol kg}^{-1}$; Mn: $0.08 \mu\text{mol kg}^{-1}$; measured October 2013; Fe: $0.52 \mu\text{mol kg}^{-1}$; Mn: $0.03 \mu\text{mol kg}^{-1}$; measured May 2013). In general, the Fe and Mn concentrations of the surface waters are lower than the concentration of the shallow pore waters, which are comparable to or lower than the concentrations of the deep groundwaters (Table 1).

4.4. Trace elements arsenic and vanadium

Arsenic concentrations in the Myrtle Grove surface waters increase between April and September, whereas the concentrations in the deeper groundwaters decrease over the same time period (Figs. 4, 5). Arsenic concentrations of the shallow pore waters at the MG-5 site proximal to the Mississippi River are comparable to those of the surface waters and deeper pore waters, whereas the As concentrations of the shallow pore waters at the MG-1 site near Barataria Bay are nearly an order of magnitude greater than either the surface waters or deeper ground-

waters during both seasons. The V concentrations of Myrtle Grove surface waters, shallow pore waters, and deep pore waters all range from 10 to 60 nmol kg^{-1} and increase between April and September, except for the V concentration of deep groundwaters at the MG-1 site, which decreases over the summer (Table 1). The subsurface peak in V concentrations generally corresponds to the depth where the subsurface Fe concentration peak occurs in the shallow pore water profiles at each site (Figs. 4, 5).

Arsenic concentrations of Myrtle Grove Canal surface waters are, on average, similar to the As concentration we measured in the Mississippi River ($14.6 \text{ nmol kg}^{-1}$, summer 2013), as well as to surface seawater As concentration ($\sim 10\text{--}20 \text{ nmol kg}^{-1}$; Middelburg et al., 1988; Cutter et al., 2001; Wurl et al., 2015). In April, V concentrations of Myrtle Grove surface waters are typical of the upper range of the Mississippi River ($4\text{--}34 \text{ nmol kg}^{-1}$; Shiller, 1997; Shiller and Mao, 2000) and similar to the V concentration measured in the Gulf of Mexico ($36 \pm 2 \text{ nmol kg}^{-1}$; Shiller and Mao, 1999). However, in September, the V concentrations of Myrtle Grove surface waters are greater than the concentrations of either the Mississippi River or the Gulf of Mexico (up to 60 nmol kg^{-1}).

4.5. Flux calculations

Calculated diffusive fluxes are shown in Table 3. The negative sign from Eq. (1) has been reversed to demonstrate that positive fluxes are moving out of the sediment and into the overlying water. These computed fluxes suggest that the shallow marsh sediments and associated pore waters are sources of Fe, Mn, and As to the surface water at both the MG-5 and MG-1 sites. Conversely, the calculated fluxes of V suggest that diffusion into the overlying water is minimal.

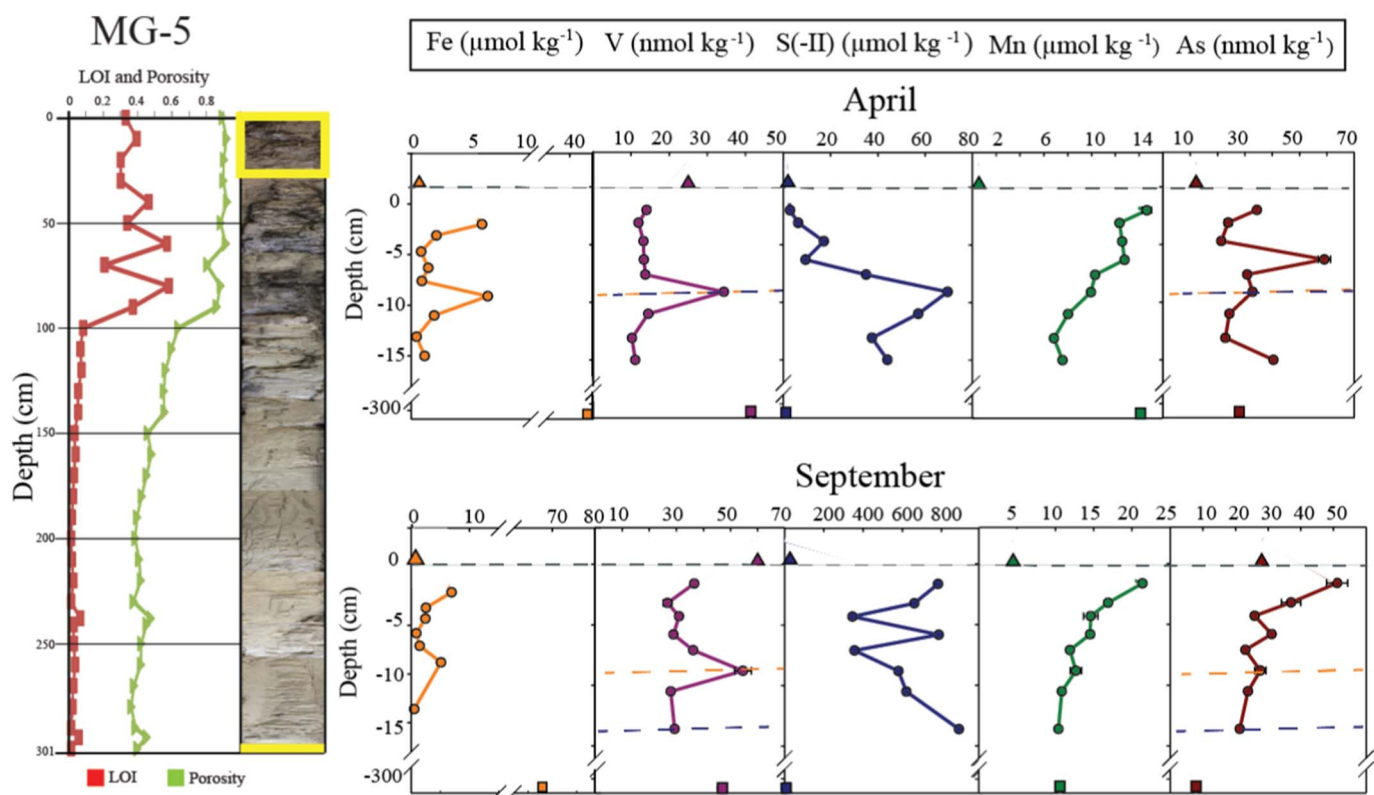


Fig. 5. Graphical summary of data presented in Table 1 for site MG-5 near the Mississippi River. The left half of the figure depicts the core image, loss on ignition (LOI) and porosity from Breaux (2015) for the length of the sediment core taken prior to piezometer emplacement. Dissolved S(-II) and trace element Fe, V, Mn, and As concentrations are shown for the surface waters in April and September (triangles), the shallow pore waters (circles), and in the deeper groundwaters (squares). The grey dashed line indicates the sediment-water interface and the orange and blue dashed lines represent dissolved Fe and S(-II) peaks, respectively. The yellow outlines on the core image indicate where pore water was extracted. (For interpretation of the references to colour in this figure legend, the reader is referred to the web version of this article.)

Instead, the predominant direction of diffusive V flux is into the sediment. Through time, Fe and Mn are exported in greater quantities in September than in April, whereas As and V fluxes are generally greater in April. Because the exact speciation of these elements is not known, the calculated fluxes are maximum estimates. For example, complexation with larger molecules (e.g., DOM) will decrease the diffusive fluxes.

5. Discussion

5.1. Marsh hydrology

Fourier analysis indicates that water level variation in the marsh most closely corresponds to tidal cycles, suggesting that water levels in the Myrtle Grove region are largely controlled by tidal forcing (Figs. 2, 3). This analysis is consistent with a conceptual groundwater model developed for Pintail Island, located in the Wax Lake Delta ~140 km to the west of our study site, where local groundwater responded most closely to tidal level, with the magnitude of the response depending on distance from the shore (O'Connor and Moffett, 2015). We note that although the tides influence the water level variability more strongly than other factors, the absolute level of water in the marsh (i.e.,

whether or not the marsh is flooded) is more relevant to redox processes affecting trace element concentrations. Kolker et al. (2013) suggested that river stage drives the flow of groundwater to the coastal bays in the lower Mississippi River Delta. At Myrtle Grove Canal, the salinity of the surface waters is less in April than in September, and combined with continuous resistivity profiling, there is evidence to support a river-derived terrestrial groundwater flux at the head of Myrtle Grove Canal, the magnitude of which is greater when river stage is high (Table 1; Breaux, 2015; Kim, 2015). Additionally, the annual cycle in the height of Canal water inundation over the marsh corresponds with the annual variability of the river stage, exhibiting markedly lower water levels in the late summer (Fig. 2A, D). Water levels in this region are also strongly affected by meteorological processes, including cold fronts that occur weekly from October to April, which causes water level fluctuations of about 0.5 m on top of existing tides. The stage of the canal, therefore, will be influenced by a combination of groundwater discharge, wind-driven coastal set-up, and tides.

5.2. Iron and sulfur cycling

The dominant processes affecting S cycling at Myrtle Grove marsh differ between the two sites. For example, when the marsh at site MG-5

Table 3

Diffusive fluxes of trace elements at each site and sampling event. Negative fluxes indicate diffusion into the sediment. Vanadium fluxes are listed first assuming all V exists as vanadyl and second assuming vanadate.

	As		Fe		Mn		V	
	MG-5	MG-1	MG-5	MG-1	MG-5	MG-1	MG-5	MG-1
April	2.3 ± 0.2	16 ± 1	4.5 · 10 ² ± 30	56 ± 6	1.1 · 10 ³ ± 80	8.3 · 10 ² ± 60	-0.98 ± 0.07, -1.0 ± 0.08	1.3 ± 0.3, 1.4 ± 0.3
September	2.9 ± 0.5	7.0 ± 0.5	7.0 · 10 ² ± 30	2.8 · 10 ⁴ ± 2 · 10 ³	1.7 · 10 ³ ± 80	4.0 · 10 ³ ± 3 · 10 ²	-2.6 ± 0.2, -2.8 ± 0.2	-1.1 ± 0.09, -1.1 ± 0.1

was flooded in September, the pore water dissolved S(–II) concentrations are > 10 times higher than in the pore water obtained when the marsh was exposed to the atmosphere, suggesting that in the absence of vegetation, tidal flooding strongly influences the shallow subsurface redox chemistry by limiting the supply of atmospheric oxygen to the shallow pore waters and initiating consumption of other electron acceptors (Miley and Kiene, 2004). In contrast to the MG-5 site, MG-1 had higher pore water S(–II) concentrations and lower water levels in April 2014 than in September 2014 (Figs. 4, 5; Table 1). We note that such seasonal differences in pore water S(–II) concentration are contrary to what other studies have reported for seasonal S(–II) variability based on *Spartina alterniflora* physiology (e.g., Krairapanond et al., 1992; Sundby et al., 2003). For example, towards the late summer and early autumn, when the growth of *Spartina alterniflora* slows, the flow of oxygen to the roots ceases and anaerobic decomposition begins (Sundby et al., 2003). Additionally, the higher temperatures in September as compared to April (28.1 °C measured at MG-1 in September vs. 22.7 °C in April) are expected to be more favorable for generating higher SO₄^{2–} reduction rates, and hence S(–II) production (Krairapanond et al., 1992; DeLaune et al., 2002; Miley and Kiene, 2004). Furthermore, Mohajerin et al. (2016) observed greater sulfide concentrations in August than in April in the upper 5 cm of pore waters collected from marsh sediments in Terrebonne Bay to the southwest of Myrtle Grove (Fig. 1). Hence, to account for the higher pore water S(–II) concentrations that were observed at the MG-1 site in April compared to September, we suggest that the seasonal differences in S(–II) concentrations at MG-1 are likely a result of removal of S(–II) through mineral precipitation or oxidation (Canfield, 1989; Morford et al., 2005; Beck et al., 2008). Dissolved S(–II) concentrations are dictated not only by rates of SO₄^{2–} reduction but also by reactive iron in the system because dissolved S(–II) reacts rapidly with Fe(II) to form Fe sulfide minerals (e.g., Rickard, 2006; Burton et al., 2011). The Fe values are much greater in the shallow pore water samples at MG-1 in September than in April. Therefore, any S(–II) produced by SO₄^{2–} reduction may have been consumed by precipitation of iron sulfide minerals like mackinawite, according to



where $\log K_{\text{FeS}} = -3.5$ for mackinawite (Delany and Lundeen, 1990; Rickard, 2006; Burton et al., 2011). The Fe²⁺ concentrations of shallow pore waters at the MG-1 site are > 400 μmol kg^{–1} in September, and the pH is ~6.6. According to Eq. (3), if all the dissolved Fe(II) in shallow pore waters at MG-1 is able to react with dissolved S(–II), only 0.8 μmol kg^{–1} S(–II) should exist in solution. Observed pore water S(–II) concentrations at MG-1 in September range from < 1 to ~9 μmol kg^{–1}, and S(–II) concentrations are lowest where the Fe concentrations are the highest (Fig. 4). Therefore, excess Fe appears to regulate the partitioning of S(–II) between dissolved and solid phases in these marsh pore waters. Indeed, geochemical modeling indicates that mackinawite is nearly saturated to over-saturated in pore waters in both April and September at both sites (Fig. 6).

Dissolved Fe concentrations are influenced not only by dissolved S(–II) but also by vegetation in the shallow subsurface (Kostka and Luther, 1995). Whereas the pore water Fe concentrations at site MG-5, which lacks vegetation, are less variable over the course of our sampling campaign (0.5–7 μmol kg^{–1}), Fe concentrations in the shallow pore waters at site MG-1, which is vegetated, increase by > 100-fold between April and September (Figs. 4, 5). Higher Fe concentrations have been observed in pore waters collected from sediments beneath vegetated marsh sites as compared to unvegetated sites during both spring and summer months (Kostka and Luther, 1995). Iron complexation with dissolved organic compounds is common in coastal waters and acts to increase its overall solubility, both by increasing the stability of Fe(III) in the aqueous phase and by ligand-induced reduction of Fe(III) to Fe(II) (Luther et al., 1992, 1996; Steinmann and Shotyk, 1997; Rose and Waite, 2003). During times of high marsh

productivity, *Spartina alterniflora* produces organic chelates that can react with solid phase Fe(III)-oxides to form Fe(III) organic complexes or reductively dissolve Fe minerals and release dissolved Fe(II), thereby increasing the effective solubility of iron (Luther et al., 1992). Therefore, as long as organic ligands are produced such that dissolved Fe concentrations are in excess of dissolved sulfide, observed Fe concentrations can still be elevated.

In contrast to the shallow pore waters the deep groundwaters have relatively low dissolved S(–II) concentrations and elevated Fe concentrations (Figs. 4, 5). This change with depth reflects the different mineralogy/composition between the shallow and deep sediments. Whereas the shallow sediments have abundant labile organic matter to fuel sulfate reduction, the deeper sediments are more mineral rich, and the low dissolved S(–II) and elevated Fe concentrations suggest that redox conditions are buffered by Fe(III) reduction in the deeper groundwaters.

5.3. Arsenic cycling

Arsenic concentrations in shallow pore waters from the MG-1 site are elevated 20 to 60 fold over the As concentrations in the underlying deeper groundwaters, 3–4 m below (Table 1). We hypothesize that the depth variation in As concentrations is related to Fe and S chemistry, in particular, iron sulfide mineral precipitation and As complexation with dissolved sulfide. Mackinawite is generally the first iron sulfide mineral to precipitate in sulfidic waters, although with time, it is commonly converted to more stable pyrite (e.g., Schoonen and Barnes, 1991a; Schoonen and Barnes, 1991b; Kirk et al., 2010). Mackinawite appears to play an important role in As cycling in the shallow sulfidic waters. Specifically, mackinawite precipitation decreases the amount of available dissolved S(–II) that can react with As(III), thereby inhibiting orpiment and/or realgar precipitation (Fig. 6; O'Day et al., 2004; Kirk et al., 2010). Second, As only adsorbs weakly onto mackinawite, which is therefore less capable of sequestering As than pyrite, which sequesters As by co-precipitation (Schoonen and Barnes, 1991a; Wolthers et al., 2005; Kirk et al., 2010; Burton et al., 2013). Furthermore, mackinawite transformation to pyrite is kinetically slower in the presence of high As and high dissolved organic carbon (DOC) concentrations (Wilkin and Ford, 2006; Wolthers et al., 2007; Kirk et al., 2010). Using loss on ignition as a proxy for sedimentary organic matter (SOM), the data suggest that SOM likely decreases with depth at both MG-1 and MG-5 sites (Figs. 4, 5). The greater As and putative SOM concentrations at the top of the core therefore suggests a positive feedback mechanism whereby formation of pyrite may be slower in the shallow subsurface. At depth, indicative of greater time for Fe-S minerals to form pyrite, As concentrations concurrently decrease (Figs. 4, 5). This suggests that, in addition to diffusion out of the shallow pore waters, As may be lost from solution owing to coprecipitation with pyrite at depth. More work is clearly needed to quantify pyritization rates and to understand As in solid phases at Myrtle Grove.

Dissolved S(–II) in Myrtle Grove pore waters can also react with As species in solution, forming thioarsenate and possible thioarsenite species (Rochette et al., 2000; Planer-Friedrich et al., 2007; Burton et al., 2013). Formation of thioarsenate species appears to increase the mobility of As in solution, and even in low sulfide waters (< 10 μmol kg^{–1}), thioarsenate species can account for a substantial portion of total aqueous As (Van der Weijden et al., 1990; O'Day et al., 2004; Bostick et al., 2005; Stauder et al., 2005; Helz and Tossell, 2008; Kirk et al., 2010; Burton et al., 2013; Couture et al., 2013). In April, the pore waters at MG-1 exhibited high dissolved S(–II) concentrations (i.e., S(–II) = 85–457 μmol kg^{–1}), and geochemical modeling indicates thioarsenate and thioarsenite species may have been present in these pore waters (Fig. 7). Conversely, for the lower sulfide concentrations measured in September pore waters from MG-1 (i.e., S(–II) < 10 μmol kg^{–1}), the arsenite oxyanion is predicted to be the dominant As(III) species, although any As(V) should have occurred as thioarse-

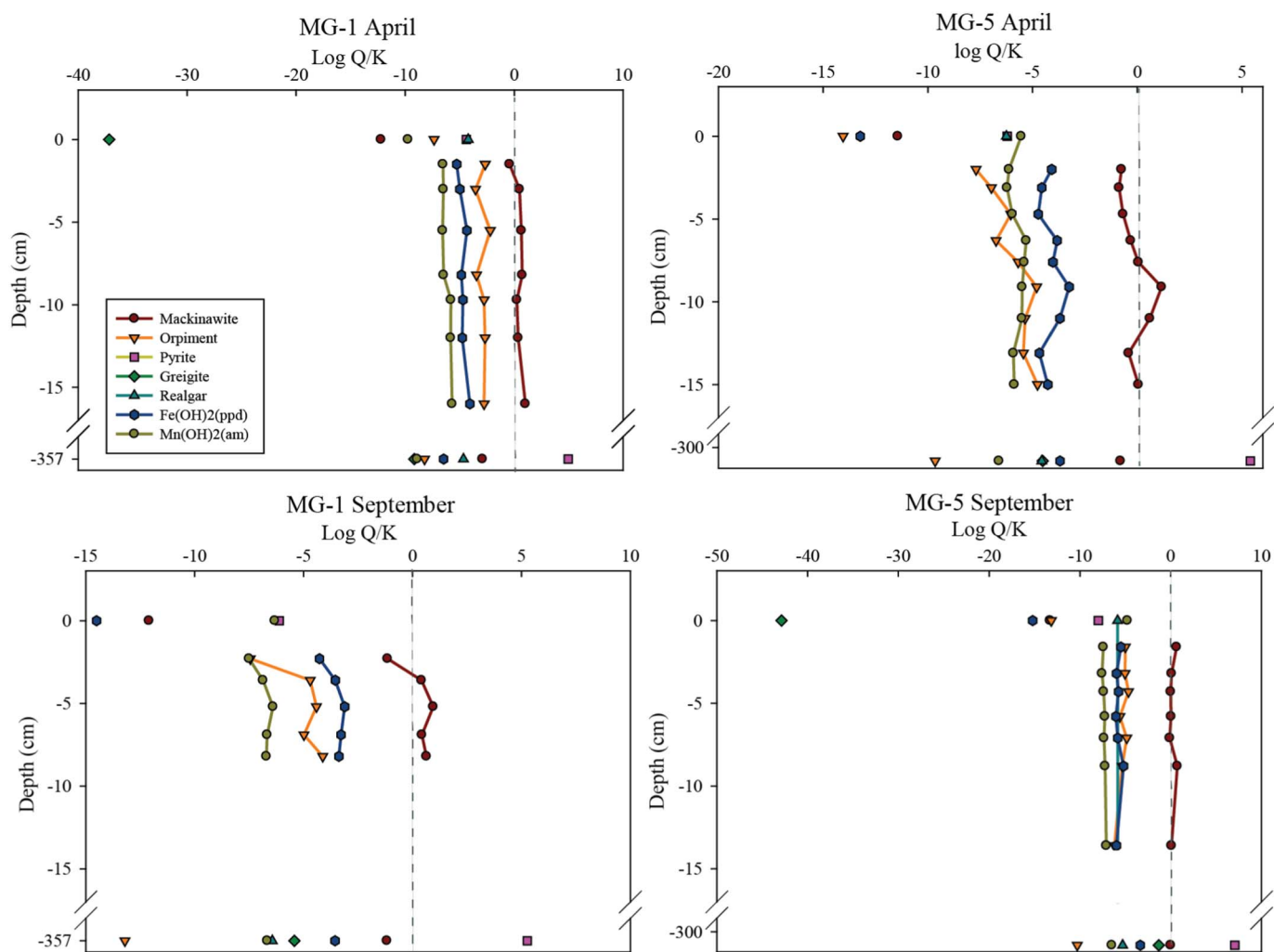


Fig. 6. Predicted mineral saturation states for Fe- and As-sulfide species in the surface waters, shallow pore waters, and deep pore waters. Because SO_4^{2-} measurements are necessary to calculate pyrite and greigite saturation, no pyrite or greigite saturation indices are available for the shallow pore waters. The saturation indices were calculated using Geochemist's Workbench® (Bethke, 2008), which employs the B-dot model to calculate activity coefficients for dissolved ions (Helgeson, 1969). The B-dot model is an extension of the Debye-Huckel theory, and is valid for predicting activity coefficients of ions in solutions of ionic strengths up to 1 m (Zhu and Anderson, 2002; Bethke, 2008). Log K values and equilibrium reactions for modeled minerals at 25 °C from the thermo.dat database in Geochemist's Workbench®:

Mineral	Reaction	Log K
Pyrite	$\text{Fe}^{2+} + \frac{7}{4}\text{HS}^- + \frac{1}{4}\text{H}^+ + \frac{1}{4}\text{SO}_4^{2-} = \text{FeS}_{2(s)} + \text{H}_2\text{O}$	-24.7
Mackinawite	$\text{Fe}^{2+} + \text{HS}^- = \text{FeS}_{(s)} + \text{H}^+$	-3.5
Orpiment	$2\text{H}_2\text{AsO}_3^- + 3\text{HS}^- + 5\text{H}^+ = \text{As}_2\text{S}_3(s) + 6\text{H}_2\text{O}$	-64.8
Realgar	$\text{H}_2\text{AsO}_3^- + \frac{9}{8}\text{HS}^- + \frac{15}{8}\text{H}^+ = \text{AsS}_{(s)} + \frac{5}{2}\text{H}_2\text{O} + \frac{1}{8}\text{SO}_4^{2-}$	-25.2
Greigite	$3\text{Fe}^{2+} + \frac{15}{4}\text{HS}^- + \frac{1}{4}\text{SO}_4^{2-} = \text{Fe}_3\text{S}_4(s) + \text{H}_2\text{O} + \frac{7}{4}\text{H}^+$	-23.4
Fe(OH) ₃ (ppd)	$\text{Fe}^{3+} + 3\text{H}_2\text{O} = \text{Fe(OH)}_3(\text{ppd}) + 3\text{H}^+$	4.89
Mn(OH) ₂ (am)	$\text{Mn}^{2+} + 2\text{H}_2\text{O} = \text{Mn(OH)}_2(\text{am}) + 2\text{H}^+$	15.3

nate species (Fig. 7). Consequently, we suggest that the statistically significant higher As concentrations measured in MG-1 shallow pore waters in April ($220 \pm 71.7 \text{ nmol kg}^{-1}$) compared to September ($152 \pm 42.8 \text{ nmol kg}^{-1}$) reflect, in part, the difference in predicted aqueous speciation of As and the potentially greater preference of thioarsenate species for the aqueous phase as compared to arsenate (*t*-test, $p < 0.05$; Table 1).

Finally, it is important to note that As is positively correlated with Mn in pore waters from both cores and that the relationship is significant for pore waters collected in September from both cores (MG-1 September $R^2 = 0.54$, $p = 0.06$; MG-5 September $R^2 = 0.94$,

$p = 0.0001$). Dissolved arsenic concentrations in natural waters are commonly associated with dissolved Fe concentrations (Sullivan and Aller, 1996; Smedley and Kinniburgh, 2002; Chaillou et al., 2003). Yet, in this system, the Mn concentrations of the pore waters are generally comparable to those of Fe. Therefore, in the shallow sediments at Myrtle Grove, As may be adsorbed to Mn mineral surfaces during times of oxygen penetration into the shallow subsurface. When conditions change to sulfidic anoxic, reductive dissolution of Mn oxides will occur, releasing As into solution, which may then form aqueous thioarsenate and/or thioarsenite complexes (Fig. 8).

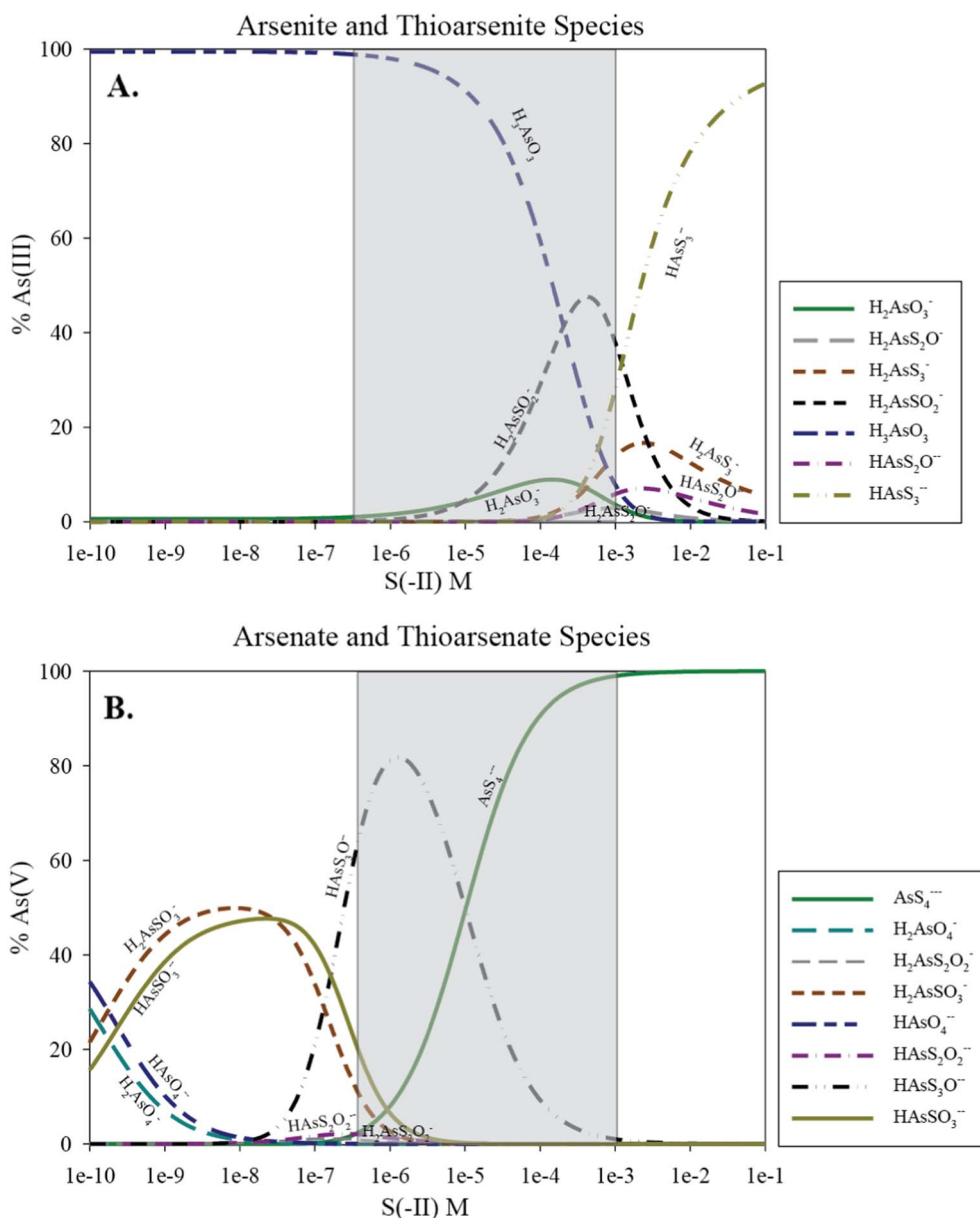


Fig. 7. Geochemical modeling prediction of As(III) (A) and As(V) (B) speciation in the presence of dissolved S(-II). The shaded region indicates the S(-II) activity observed at Myrtle Grove. The average pH (7.0) and average As concentration (100 nmol kg^{-1}) of pore water samples were used to construct the diagram. The equilibrium constants for thioarsenate and thioarsenite formation are summarized in Table 2 of Yang et al. (2015).

5.4. Vanadium cycling

Under iron- and sulfate-reducing conditions, such as those observed in Myrtle Grove shallow pore waters and deeper groundwaters, V should exist as a V(IV) or potentially V(III) species (Wehrli and Stumm, 1989; Wright and Belitz, 2010). These redox states are generally less soluble compared to V(V), the predominant redox state in oxidized surface waters (Wanty and Goldhaber, 1992; Wright et al., 2014). Nonetheless, V concentrations do not vary systematically with depth at Myrtle Grove (Figs. 4, 5). In the shallow pore waters, the V peak corresponds closely with that of Fe, and V and Fe are significantly correlated, suggesting that similar geochemical processes control their aqueous concentrations ($R^2 = 0.50$; $p < 0.005$). Given the high organic matter content of the shallow sediments (> 80%), it is likely that dissolved organic matter complexes with aqueous V, thereby increasing its solubility in a manner similar to that of Fe (Beck et al., 2008; Pourret et al., 2012). Even in groundwaters with low dissolved organic carbon, V solubility may be enhanced through complexation

with DOC (Telfeyan et al., 2015).

A comparison of Fe and V in the deeper groundwaters, however, reveals that, although the V trend generally follows that of Fe, the magnitude is much less. More specifically, the Fe concentrations of the deep groundwater are up to 30 times greater than in the average pore water concentrations, whereas the increase in V is much less (up to 2.7 times). Therefore, although Fe and V behave very similarly in the shallow subsurface, their concentrations are decoupled at depth. The disconnect between Fe and V behavior at depth may reflect their different reactivities to sulfur. Elevated Fe concentrations at depth are indicative of Fe(III) oxide/oxyhydroxide reduction to more soluble Fe(II), and without elevated S(-II) concentrations, Fe mobility will increase (e.g., Luther et al., 1992). Because V does not positively covary with Fe in deep pore waters (~3–4 m), V may not be initially adsorbed/desorbed to Fe(III) oxides/hydroxides at depth (e.g., Hem, 1977; Peacock and Sherman, 2004). Alternatively, V may initially adsorb to Fe/Mn oxides/hydroxides and upon reductive dissolution of Fe(III) oxides/hydroxides, V may be released to solution and subse-

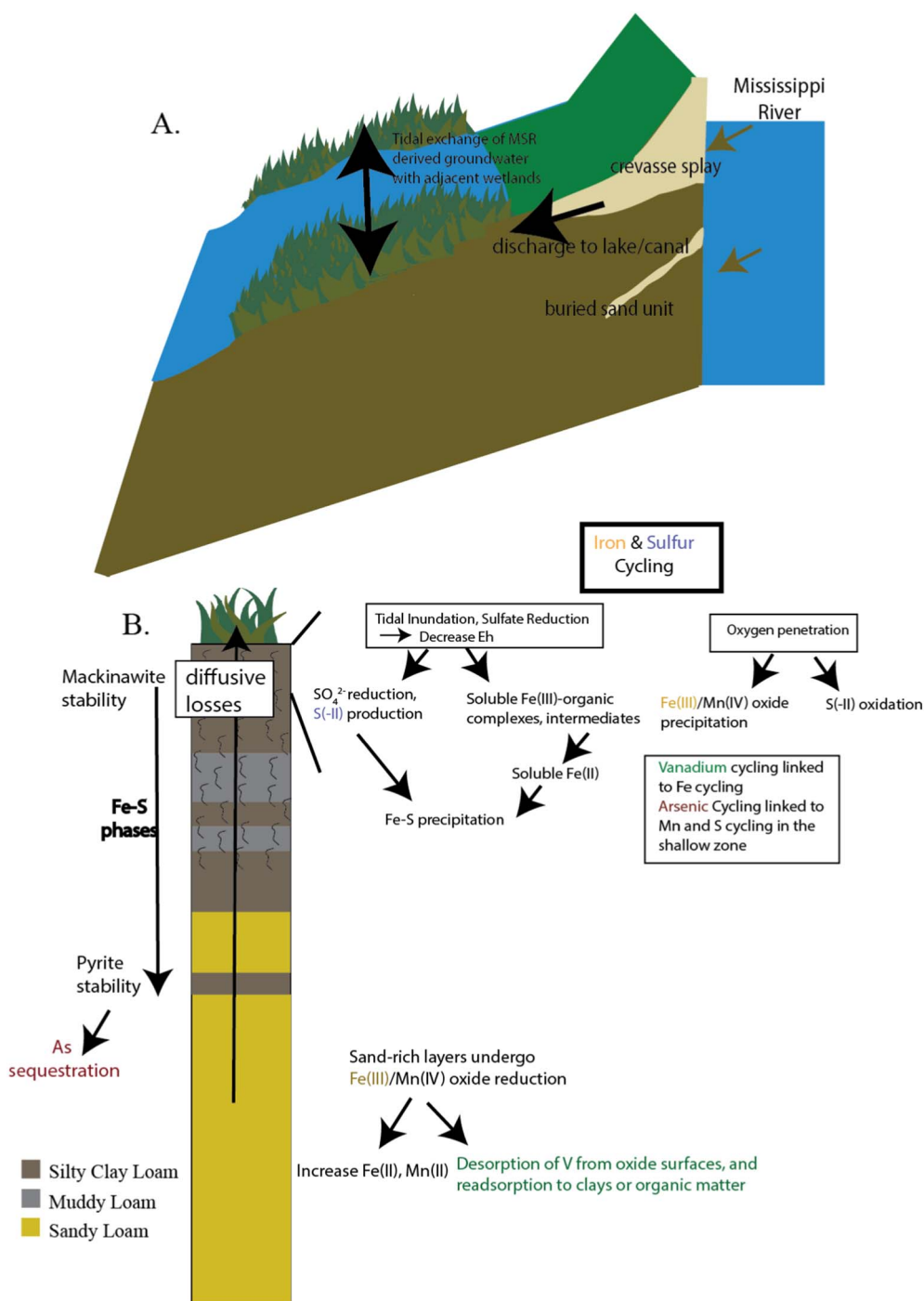


Fig. 8. Summary of hypothesized hydrologic (A) and chemical (B) processes affecting trace element fluxes as discussed in the text. MSR: Mississippi River.

quently adsorbed to surfaces of other minerals or sedimentary organic matter (Fig. 8). In addition to Fe(III) oxides/hydroxides, V may adsorb to humics or more weakly to clays (McBride, 1978; McBride, 1979; Wanty and Goldhaber, 1992). Whereas the surficial sediments have abundant labile organic matter, the deeper sediments likely contain more recalcitrant organic matter less susceptible to degradation. Therefore, V may be associated with the solid phase organic matter at depth as opposed to forming the dissolved organic complexes in the shallow pore waters.

5.5. Diffusive pore water fluxes of trace elements

Positive fluxes of Mn, Fe, and As suggest that the coastal marsh pore

waters act as a source of these trace elements to the coastal bay waters (Table 3). These results are consistent with observations that positive diffusive fluxes of Fe, Mn, and As from sediments occur under reducing conditions, and the fluxes are similar to those at other sites (Table 4; Li et al., 2014). Of the elements studied in Myrtle Grove marsh pore waters, Fe concentrations vary the most through time and space, reflecting the coupling of Fe and S cycling and the dependence of aqueous Fe concentrations on iron sulfide mineral precipitation. Although V concentrations of pore waters from Myrtle Grove appear to be coupled to Fe cycling, diffusive fluxes of V are directed into the sediments. The negative V fluxes represent the greater V concentrations in Myrtle Grove surface waters compared to pore water concentrations (Tables 1, 3).

Table 4

Summary of diffusive fluxes calculated at other study sites. Negative signs indicate the flux is directed into the sediment.

Element	Study area	Diffusional flux nmol cm ⁻² yr ⁻¹	Reference
As	Myrtle Grove marsh	2.1–17	This study
	Lagoons, Venice, Italy	2.19, – 1.58	Turetta et al. (2005)
	Danshuei Estuary, Taiwan	0.627–4.67	Fang and Chen (2015)
	Amazon Shelf	0.292–91.3	Sullivan and Aller (1996)
	Bay of Biscay, France	1.00–2.00	Chaillou et al. (2003)
Fe	Myrtle Grove marsh	50–30,000	This study
	Lagoons, Venice, Italy	– 30.7, – 55.2	Turetta et al. (2005)
	Gulf of Finland;	182.5–36,500	Pakhomova et al. (2007)
	Vistua Lagoon, Baltic Sea;		
	Golubaya Bay; Black Sea		
	Galveston Bay, Texas	256–3431	Warnken et al. (2001)
	Lake Bret, Switzerland	315–78,8400	Belzile et al. (1996)
	Rosário salt marsh, Portugal	0.0105, – 0.051	Santos-Echeandía et al. (2010)
	Iberian Peninsula salt marshes	– 16,870–2834	Blasco et al. (2000)
	Myrtle Grove marsh	770–4,300	This study
Mn	Vistua Lagoon, Baltic Sea; Golubaya Bay; Black Sea	2560–16,2000	Pakhomova et al. (2007)
	Galveston Bay, Texas	730–13,400	Warnken et al. (2001)
	Lake Bret, Switzerland	378–1480	Belzile et al. (1996)
	Rosário salt marsh, Portugal	4800, 290	Santos-Echeandía et al. (2010)
	Iberian Peninsula salt marshes	61.7–3831	Blasco et al. (2000)
V	Myrtle Grove marsh	– 3.0–1.7	This study
	Vigio Ria, Spain	1.48–4.35	Santos-Echeandía et al. (2009)
	Lagoons, Venice, Italy	– 73.6, 11.4	Turetta et al. (2005)

The fluxes reported here represent maximum estimates because we have calculated the diffusive flux of solutes. The real magnitudes are dependent upon the frequency with which the marsh is flooded and subsequently flushed (Santos-Echeandía et al., 2010). The enriched water must be flushed from the marsh before reprecipitation of iron oxides or iron sulfides occurs. A portion of the diffusive flux may therefore be recirculated at the sediment-water interface (Chaillou et al., 2003). From the time series analysis of the hydrologic variables, it is likely that the marsh is flooded more frequently during the spring, which would suggest that diffusive fluxes are more relevant during this time.

To consider the significance of these trace element (i.e., As, V) diffusive fluxes from the sediments to the overlying water column within Barataria Bay, a comparison with estimated reservoir fluxes is useful. Previous work separated hydrologic fluxes into (Q_{in}) and out of (Q_{out}) Barataria Bay, and the pertinent values are summarized in Table 5 (Kolker et al., 2013). If we assume that the concentrations of As and V in the water column of Barataria Bay can be considered to represent a balance between the fluxes of both trace elements transported into the bay from the Gulf of Mexico (i.e., the tidal prism), surface water runoff, submarine groundwater discharge, input from the Davis Pond Freshwater Diversion, meteoric precipitation over the

marsh, and diffusive fluxes, and assuming the Bay is under steady-state conditions, then,

$$Q_{out} \times [TM]_{BB} = Q_{TP} \times [TM]_{GoM} + Q_{surf} \times [TM]_{MG-1} + Q_{DPFD} \times [TM]_{MG-1} + Q_{net\ rain} \times [TM]_{rain} + Q_{SGD} \times [TM]_{MG-1} + Diff. Flux \quad (4)$$

in which $[TM]_{BB}$ is the concentration of the trace metal (i.e., As or V) in Barataria Bay, Q_{TP} is the flux of water from the tidal prism, $[TM]_{GoM}$ is the trace metal concentration in the Gulf of Mexico, Q_{surf} is the flux of various surface water sources, $[TM]_{MG-1}$ is the average trace metal concentration measured in the surface water at MG-1, Q_{DPFD} is the flux of water from the Davis Pond Freshwater Diversion, $Q_{net\ rain}$ is the flux of rainwater minus the evaporative flux, $[TM]_{rain}$ is the trace metal concentration of the rain, which is considered negligible given the low concentration in rain and orders of magnitude lower flux of rain compared to the other fluxes, and Q_{SGD} is the flux of submarine groundwater discharge to Barataria Bay (Kolker et al., 2013). Q_{out} represents the flux exiting the bay on the ebb tide and is determined from a salinity balance, such that

Table 5

Values used in mass balance calculation.

Flux	Source	Value
SGD (m ³ /day)	Groundwater discharge ^a	1.28–1.35 × 10 ⁸ (with and without DPFD)
Rainwater flux (m ³ /day) ^a		2.46 × 10 ⁶
Evaporative flux (m ³ /day) ^a		1.87 × 10 ⁶
Q_{surf} (m ³ /day) ^{a,d}	Unregulated surface fluxes	1.73 × 10 ⁷
As_{MG-1} (nmol/m ³)	Average As MG-1 surface water	1.42 × 10 ⁴
V_{MG-1} (nmol/m ³)	Average V MG-1 surface water	2.87 × 10 ⁴
Q_{TP} (m ³ /day)	Tidal Prism ^a	2.3 × 10 ⁸
As_{GoM} (nmol/m ³)	Average seawater (see Section 4.4)	1.5 × 10 ⁴
V_{GoM} (nmol/m ³)	Gulf of Mexico concentration ^c	3.6 × 10 ⁴
DPFD (m ³ /day) ^{a,c}	Davis Pond Freshwater Diversion	7.78 × 10 ⁶
Area of Barataria Bay (cm ²) ^b		5.7 × 10 ¹²

^a Values from Kolker et al. (2013)^b Value from Feng and Li (2010)^c Value from Shiller and Mao (1999)^d Value from Reed (1995)^e Value from Allison et al. (2012)

$$Q_{out} = Q_{in} \left(\frac{\text{salinity flood tide}}{\text{salinity ebb tide}} \right) \quad (5)$$

in which Q_{in} is the flux from the tidal prism and the salinities of the flood and ebb tides are 25 and 15, respectively (Kolker et al., 2013). The Q_{out} flux is therefore $3.83 \times 10^8 \text{ m}^3 \text{ day}^{-1}$. The diffusive flux considers the maximum and minimum flux estimates for the trace metals. The diffusive fluxes of As and V from Table 3 are multiplied by the area of the bay to yield a range of 3.3×10^{10} to $2.7 \times 10^{11} \text{ nmol day}^{-1}$ directed out of the sediments for As and a range of $4.7 \times 10^{10} \text{ nmol day}^{-1}$ directed into the sediments to $2.7 \times 10^{10} \text{ nmol day}^{-1}$ directed out of the sediments for V. Eq. (4) can therefore be solved for the As and V concentrations in Barataria Bay, which are computed to range from 1.48×10^4 to $1.53 \times 10^4 \text{ nmol m}^{-3}$ for As and 3.29×10^4 to $3.31 \times 10^4 \text{ nmol m}^{-3}$ for V. The range is determined by computing the sum with and without the DPF and accounting for both the minimum and maximum estimates of the diffusive fluxes. The computed V concentration range for Barataria Bay is less than the concentration of the Gulf and greater than the concentration in Myrtle Grove Canal, which is consistent with the results of the diffusive fluxes that suggest that the marsh at Myrtle Grove serves as a sink for V. The As concentration of seawater and of Myrtle Grove Canal are very similar, and the estimated As concentration range of Barataria Bay is within the range of these two reservoirs. Because the uncertainty of this estimate is likely greater than the variation between the As concentrations of the reservoirs, it is difficult to conclude whether the diffusive fluxes contribute substantially to either. However, the upper end of the estimated As concentration for Barataria Bay is slightly greater than either reservoir, which is consistent with a diffusive input from the sediments.

6. Conclusions

- River stage and subsequent groundwater discharge at the head of Myrtle Grove drives long-term (annual) variation in water level, whereas tidal variation appears to be the strongest hydrologic force affecting Myrtle Grove pore waters on shorter time scales. In the absence of vegetation, tidal flooding depletes oxygen levels and drives sulfate reduction in the shallow subsurface.
- Arsenic aqueous speciation and partitioning between aqueous and sediment phases is linked to S(–II) cycling in the shallow pore waters. Correlation analysis also suggests that As may be associated with Mn. The As concentrations in the shallow pore waters proximal to Barataria Bay are elevated compared to surface or deep pore waters, but more work is needed to determine the observed spatial distribution.
- Vanadium in shallow pore waters correlates with Fe concentrations. This relationship may be due, in part, to complexation of both Fe and V with dissolved organic complexes, which are likely abundant in the shallow subsurface. At depth, however, V and Fe concentrations are decoupled. Upon reductive dissolution of Fe(III) oxides/oxyhydroxides, V may be released from solution and adsorbed to other mineral surfaces (i.e., clay) or recalcitrant SOM.
- The diffusive flux calculations suggest that shallow pore waters of the Myrtle Grove marsh have the potential to act as a supply of Fe, Mn, and As to Barataria Bay and ultimately the Gulf of Mexico, whereas V is sequestered in the sediments. Incorporating these diffusive fluxes of As and V into a mass balance for Barataria Bay also suggests that the V is lost from the water column to the sediments, whereas the sediments serve as a source of As to Barataria Bay. The effective diffusive flux will depend on the frequency and duration at which the marsh is flooded.

Supplementary data to this article can be found online at <http://dx.doi.org/10.1016/j.marchem.2017.03.010>.

Acknowledgements

This work was funded by NSF grant EAR-1141692 to K. H. Johannesson, NSF grant EAR-1141716 to A. S. Kolker, NSF grant EAR-1141685 to J. E. Cable, and the Vokes Fellowship from Tulane University Earth and Environmental Sciences Department. We would also like to thank Dr. Dave Burdige for assistance with determining fluxes, Alex Ameen for field assistance and Myrtle Grove Marina for dock use. We thank two anonymous reviewers and AE, William Landing, whose comments greatly improved this paper.

References

- Aller, R.C., 1982. The effects of macrobenthos on chemical properties of marine sediment and overlying water. In: *Animal-Sediment Relations*. Springer US, pp. 53–102.
- Allison, M.A., Demas, C.R., Ebersole, B.A., Kleiss, B.A., Little, C.D., Meselhe, E.A., Powell, N.J., Pratt, T.C., Vosburg, B.M., 2012. A water and sediment budget for the lower Mississippi-Atchafalaya River in flood years 2008–2010: implications for sediment discharge to the oceans and coastal restoration in Louisiana. *J. Hydrol.* 432–433, 84–97.
- American Public Health Association, American Water Works Association, Water Environment Federation, 1985. *Standard Methods for the Examination of Water and Wastewater*, 16th ed. (Washington DC, USA).
- Báez-Cazull, S.E., McGuire, J.T., Cozzarelli, I.M., Voytek, M.A., 2008. Determination of dominant biogeochemical processes in a contaminated aquifer-wetland system using multivariate statistical analysis. *J. Environ. Qual.* 37, 30–46.
- Basu, A.R., Jacobsen, S.B., Poreda, R.J., Dowling, C.B., Aggarwal, P.K., 2001. Large groundwater strontium flux to the oceans from the bengal basin and the marine strontium isotope record. *Science* 293, 1470–1473.
- Beck, M., Dellwig, L., Schnetger, B., Brumsack, H.J., 2008. Cycling of trace metals (Mn, Fe, Mo, U, V, Cr) in deep pore waters of intertidal flat sediments. *Geochim. Cosmochim. Acta* 72, 2822–2840.
- Beck, A.J., Cochran, J.K., Sañudo-Wilhelmy, S.A., 2010. The distribution and speciation of dissolved trace metals in a shallow subterranean estuary. *Mar. Chem.* 121 (1), 145–156.
- Belzile, N., Pizarro, J., Filella, M., Buffle, J., 1996. Sediment diffusive fluxes of Fe, Mn, and P in a eutrophic lake: contribution from lateral vs bottom sediments. *Aquat. Sci.* 58 (4), 327–354.
- Berner, R.A., 1980. *Early Diagenesis*. Princeton University Press, Princeton, NJ (241 pp).
- Bethke, C.M., 2008. *Geochemical and Biogeochemical Reaction Modeling*, second ed. Cambridge University Press.
- B'hymer, C., Caruso, J.A., 2004. Arsenic and its speciation analysis using high-performance liquid chromatography and inductively coupled plasma mass spectrometry. *J. Chromatogr. A* 1045, 1–13.
- Bianchi, T.S., Wysocki, L.A., Schreiner, K.M., Filley, T.R., Corbett, D.R., Kolker, A.S., 2011a. Sources of terrestrial organic carbon in the Mississippi River Plume Region: evidence for the importance of coastal marsh inputs. *Aquat. Geochim.* 17, 431–456.
- Bianchi, T.S., Cook, R.L., Perdue, E.M., Kolic, P.E., Green, N., Zhang, Y., Smith, R.W., Kolker, A.S., Ameen, A., King, G., Ojwang, L.M., 2011b. Impacts of diverted freshwater on dissolved organic matter and microbial communities in Barataria Bay, Louisiana, USA. *Mar. Environ. Res.* 72 (5), 248–257.
- Blasco, J., Saenz, V., Gómez-Parra, A., 2000. Heavy metal fluxes at the sediment-water interface of three ecosystems from south-west of the Iberian peninsula. *Sci. Total Environ.* 247 (2), 189–199.
- Bone, S.E., Gonnea, M.E., Charette, M.A., 2006. Geochemical cycling of arsenic in a coastal aquifer. *Environ. Sci. Technol.* 40, 3273–3278.
- Bostick, B.C., Fendorf, S., Brown, G.E., 2005. In situ analysis of thioarsenite complexes in neutral to alkaline arsenic sulphide solutions. *Mineral. Mag.* 69, 781–795.
- Breaux, A.M., 2015. *Utilization of Shallow Seismic, Resistivity Profiling, and Sediment Core Analyses for Identification of Semi-Permeable Sediments That Act as Conduits for Submarine Groundwater Discharge, Barataria Bay, Louisiana*. Tulane University, Master's Thesis.
- Breit, G.N., Wanty, R.B., 1991. Vanadium Accumulation in Carbonaceous Rocks: A Review of Geochemical Controls during Deposition and Diagenesis. 91. pp. 83–97.
- Burdige, D.J., 1993. The biogeochemistry of manganese and iron reduction in marine sediments. *Earth Sci. Rev.* 35, 249–284.
- Burdige, D.J., 2006. *Geochemistry of Marine Sediments*. Vol. 398 Princeton University Press, Princeton.
- Burton, E.D., Bush, R.T., Johnston, S.G., Sullivan, L.A., Keene, A.F., 2011. Sulfur biogeochemical cycling and novel Fe-S mineralization pathways in a tidally re-flooded wetland. *Geochim. Cosmochim. Acta* 75, 3434–3451.
- Burton, E.D., Johnston, S.G., Planer-Friedrich, B., 2013. Coupling of arsenic mobility to sulfur transformations during microbial sulfate reduction in the presence and absence of humic acid. *Chem. Geol.* 343, 12–24.
- Cable, J.E., Bugna, G.C., Burnett, W.C., Chanton, J.P., 1996. Application of Rn-222 and CH₄ for assessment of groundwater discharge to the coastal ocean. *Limnol. Oceanogr.* 41, 1347–1353.
- Cai, W.J., Wang, Y., Krest, J., Moore, W.S., 2003. The geochemistry of dissolved inorganic carbon in a surficial groundwater aquifer in north inlet, South Carolina, and the carbon fluxes to the coastal ocean. *Geochim. Cosmochim. Acta* 67 (4), 631–639.
- Canfield, D.E., 1989. Reactive iron in marine-sediments. *Geochim. Cosmochim. Acta* 53, 619–632.
- Cantley, L.C., Aisen, P., 1979. Fate of cytoplasmic vanadium—implications on (Na,K)-ATPase inhibition. *J. Biol. Chem.* 254, 1781–1784.
- Carey, E., Taillefert, M., 2005. The role of soluble Fe(III) in the cycling of iron and sulfur

- in coastal marine sediments. *Limnol. Oceanogr.* 50, 1129–1141.
- Chaillou, G., Schäfer, J., Anschutz, P., Lavaux, G., Blanc, G., 2003. The behavior of arsenic in muddy sediments of The Bay of Biscay (France). *Geochim. Cosmochim. Acta* 67 (16), 2993–3003.
- Charette, M.A., Sholkovitz, E.R., 2006. Trace element cycling in a subterranean estuary: part 2. Geochemistry of the pore water. *Geochim. Cosmochim. Acta* 70, 811–826.
- Charette, M.A., Gonneea, M.E., Morris, P.J., Statham, P., Fones, G., Planquette, H., Salter, I., Garabato, A.N., 2007. Radium isotopes as tracers of iron sources fueling a southern ocean phytoplankton bloom. *Deep-Sea Res. II Top. Stud. Oceanogr.* 54, 1989–1998.
- Chevis, D.A., Johannesson, K.H., Burdige, D.J., Tang, J., Moran, S.B., Kelly, R.P., 2015a. Submarine groundwater discharge of rare earth elements to a tidally-mixed estuary in southern Rhode Island. *Chem. Geol.* 397, 128–142.
- Chevis, D.A., Johannesson, K.H., Burdige, D.J., Cable, J.E., Martin, J.B., Roy, M., 2015b. Rare earth element cycling in a sandy subterranean estuary in Florida, USA. *Mar. Chem.* 176, 34–50.
- Couture, R.M., Rose, J., Kumar, N., Mitchell, K., Wallschläger, D., Van Cappellen, P., 2013. Sorption of arsenite, arsenate, and thioarsenates to iron oxides and iron S(–II) s: a kinetic and spectroscopic investigation. *Environ. Sci. Technol.* 47, 5652–5659.
- Couvillion, B.R., Barras, J.A., Steyer, G.D., Sleavin, W., Fischer, M., Beck, H., Trahan, N., Griffin, B., Heckman, D., 2011. Land Area Change in Coastal Louisiana From 1932 to 2010. U.S. Geological Survey Scientific Investigations Map 3164. (12p).
- Craven, D.B., Jahnke, R.A., Carlucci, A.F., 1986. Fine-scale vertical distributions of microbial biomass activity in California borderland sediments. *Deep-Sea Res. Part A* 33, 379–390.
- CRMS, Coastal Protection and Restoration Authority (CPRA) of Louisiana, 2015. Coastwide Reference Monitoring System-Wetlands Monitoring Data. Retrieved from Coastal Information Management System (CIMS) database. <http://cims.coastal.louisiana.gov> (Accessed 14 April 2015).
- Cullen, W.R., Reimer, K.J., 1989. Arsenic speciation in the environment. *Chem. Rev.* 89, 713–764.
- Cutter, G.A., Cutter, L.S., Featherstone, A.M., Lohrenz, S.E., 2001. Antimony and arsenic biogeochemistry in the western Atlantic Ocean. *Deep-Sea Res. II Top. Stud. Oceanogr.* 48, 2895–2915.
- Das, A., Justic, D., Swenson, E., 2010. Modeling estuarine-shelf exchanges in a deltaic estuary: implications for coastal carbon budgets and hypoxia. *Ecol. Model.* 221, 978–985.
- Das, A., Justic, D., Inoue, M., Hoda, A., Huang, H.S., Park, D.H., 2012. Impacts of MSR diversions on salinity gradients in a deltaic Louisiana estuary: ecological and management implications. *Estuar. Coast. Shelf Sci.* 111, 17–26.
- Datta, S., Neal, A.W., Mohajerin, T.J., Ocheltree, T., Rosenheim, B.E., White, C.D., Johannesson, K.H., 2011. Perennial ponds are not an important source of water or dissolved organic matter to groundwaters with high arsenic concentrations in West Bengal, India. *Geophys. Res. Lett.* 38, L20404.
- Day Jr., J.W., Boesch, D.F., Clairain, E.J., Kemp, G.P., Laska, S.B., Mitsch, W.J., Orth, K., Mashriqui, H., Reed, D.J., Shabman, L., Simenstad, C.A., Streever, B.J., Twilley, R.R., Watson, C.C., Wells, J.T., Whigham, D.F., 2007. Restoration of the Mississippi Delta: lessons from hurricanes Katrina and Rita. *Science* 315 (5819), 1679–1684.
- Delany, J.M., Lundeen, S.R., 1990. The LLNL thermochemical database. In: Lawrence Livermore National Laboratory Report UCRL-21658. Lawrence Livermore National Laboratory.
- DeLaune, R.D., Devai, I., Crozier, C.R., Kelle, P., 2002. Sulfate reduction in Louisiana marsh soils of varying salinities. *Commun. Soil Sci. Plant Anal.* 33, 79–94.
- DeLaune, R.D., Jugsujinda, A., Peterson, W.H., 2003. Impacts of Mississippi River freshwater introduction on enhancing marsh accretionary processes in a Louisiana estuary. *Estuar. Coast. Shelf Sci.* 58, 653–662.
- Duan, L.Q., Song, J.M., Li, X.G., Yuan, H.M., 2010. The behaviors and sources of dissolved arsenic and antimony in Bohai Bay. *Cont. Shelf Res.* 30, 1522–1534.
- Eary, L.E., 1992. The solubility of amorphous As₂S₃ from 25 to 90 °C. *Geochim. Cosmochim. Acta* 56, 2267–2280.
- Eaton, A.D., 2005. SULFATE (4500-SO42-)/Turbidimetric Method. Standard Methods for the Examination of Water and Wastewater, 21st ed. American Public Health Association, Washington, DC.
- Eaton, A.D., Clesceri, L.S., Greenberg, A.E., 1995. S(–II) (4500-S2 –)/Methylene Blue Method. Standard Methods for the Examination of Water and Wastewater, 19th ed. American Public Health Association, Washington, DC (pp. 4–122–4–123).
- Fagherazzi, S., Wiberg, P.L., Temmerman, S., Stuyf, E., Zhao, Y., Raymond, P.A., 2013. Fluxes of water, sediments, and biogeochemical compounds in salt marshes. *Ecol. Process.* 2 (3).
- Fang, T., Chen, Y., 2015. Arsenic speciation and diffusion flux in Danshuei Estuary sediments, Northern Taiwan. *Mar. Pollut. Bull.* 101, 98–109.
- Fendorf, S., Michael, H.A., van Geen, A., 2010. Spatial and temporal variations of groundwater arsenic in South and Southeast Asia. *Science* 328 (5982), 1123–1127.
- Feng, Z., Li, C., 2010. Cold-front-induced flushing of the Louisiana Bays. *J. Mar. Syst.* 82 (4), 252–264.
- Fiorentino, C.E., Paoloni, J.D., Sequeira, M.E., Arosteguy, P., 2007. The presence of vanadium in groundwater of southeastern extreme the pampean region Argentina: relationship with other chemical elements. *J. Contam. Hydrol.* 93 (1), 122–129.
- Froelich, P., Klinkhammer, G.P., Bender, M.A.A., Luedtke, N.A., Heath, G.R., Cullen, D., Maynard, V., 1979. Early oxidation of organic matter in pelagic sediments of the eastern equatorial Atlantic: suboxic diagenesis. *Geochim. Cosmochim. Acta* 43 (7), 1075–1090.
- Gaillard, J.F., Pauwels, H., Michard, G., 1989. Chemical diagenesis in coastal marine sediments. *Oceanol. Acta* 12, 175–187.
- Gleeson, J., Santos, I.R., Maher, D.T., Golsby-Smith, L., 2013. Groundwater-surface water exchange in a mangrove tidal creek: evidence from natural geochemical tracers and implications for nutrient budgets. *Mar. Chem.* 156, 27–37.
- Goldschmidt, V.M., 1954. *Geochemistry*. Clarendon Press, Oxford.
- Gonneea, M.E., Charette, M.A., Liu, Q., Herrera-Silveira, J.A., Morales-Ojeda, S.M., 2014. Trace element geochemistry of groundwater in a karst subterranean estuary (Yucatan Peninsula, Mexico). *Geochim. Cosmochim. Acta* 132, 31–49.
- Helgeson, H.C., 1969. Thermodynamics of hydrothermal systems at elevated temperatures and pressures. *Am. J. Sci.* 267, 729–804.
- Hellwegger, F.L., Farley, K.J., Lall, U., Di Toro, D.M., 2003. Greedy algae reduce arsenate. *Limnol. Oceanogr.* 48, 2275–2288.
- Helz, G.R., 2014. Activity of zero-valent sulfur in sulfidic natural waters. *Geochem. Trans.* 15, 13.
- Helz, G.R., Tossell, J.A., 2008. Thermodynamic model for arsenic speciation in sulfidic waters: a novel use of ab initio computations. *Geochim. Cosmochim. Acta* 72, 4457–4468.
- Hem, J.D., 1977. Reactions of metal ions at surfaces of hydrous iron-oxide. *Geochim. Cosmochim. Acta* 41, 527–538.
- Hollibaugh, J.T., Carini, S., Gürleyük, H., Jellison, R., Joye, S.B., LeCleir, G., Meile, C., Vasquez, L., Wallschläger, D., 2005. Arsenic speciation in Mono Lake, California: response to seasonal stratification and anoxia. *Geochim. Cosmochim. Acta* 69 (8), 1925–1937.
- Hughes, C.E., Binning, P., Willgoose, G.R., 1998. Characterisation of the hydrology of an estuarine wetland. *J. Hydrol.* 211, 34–49.
- Hunt, R.J., Krabbenhoft, D.P., Anderson, M.P., 1997. Assessing hydrogeochemical heterogeneity in natural and constructed wetlands. *Biogeochemistry* 39, 271–293.
- Inoue, M., Park, D., Justic, D., Wiseman, W.J., 2008. A high-resolution integrated hydrology-hydrodynamic model of the Barataria Basin system. *Environ. Model. Softw.* 23, 1122–1132.
- Jay, J.A., Blute, N.K., Hemond, H.F., Durant, J.L., 2004. Arsenic-sulfides confound anion exchange resin speciation of aqueous arsenic. *Water Res.* 38, 1155–1158.
- Jeandel, C., Caisso, M., Minster, J.F., 1987. Vanadium behaviour in the global ocean and in the Mediterranean Sea. *Mar. Chem.* 21 (1), 51–74.
- Johannesson, K.H., Burdige, D.J., 2007. Balancing the global oceanic neodymium budget: evaluating the role of groundwater. *Earth Planet. Sci. Lett.* 253, 129–142.
- Johannesson, K.H., Tang, J.W., Daniels, J.M., Bounds, W.J., Burdige, D.J., 2004. Rare earth element concentrations and speciation in organic-rich blackwaters of the Great Dismal Swamp, Virginia, USA. *Chem. Geol.* 209, 271–294.
- Johannesson, K.H., Chevis, D.A., Burdige, D.J., Cable, J.E., Martin, J.B., Roy, M., 2011. Submarine groundwater discharge is an important net source of light and middle REEs to the coastal waters of the Indian River Lagoon, Florida, USA. *Geochim. Cosmochim. Acta* 75 (3), 825–843.
- Kim, J., 2015. Investigating Groundwater Inputs to Mississippi River Deltaic Wetlands Using Spatial and Temporal Responses of the Geochemical Tracer, 222Rn. Master's Thesis. University of North Carolina, Chapel Hill.
- Kim, G., Ryu, J., Yang, H., Yun, S., 2005. Submarine groundwater discharge (SGD) into the Yellow Sea revealed by 228Ra and 226Ra isotopes: implications for global silicate fluxes. *Earth Planet. Sci. Lett.* 237, 156–166.
- Kirk, M.F., Roden, E.E., Crossey, L.J., Brearley, A.J., Spilde, M.N., 2010. Experimental analysis of arsenic precipitation during microbial sulfate and iron reduction in model aquifer sediment reactors. *Geochim. Cosmochim. Acta* 74, 2538–2555.
- Kirman, Z.D., Sericano, J.L., Wade, T.L., Bianchi, T.S., Marcantonio, F., Kolker, A.S., 2016. Composition of depth distribution of hydrocarbons in Barataria Bay marsh sediments after the deepwater horizon oil spill. *Environ. Pollut.* 214, 101–113.
- Kolker, A.S., Allison, M.A., Hameed, S., 2011. An evaluation of subsidence rates and sea-level variability in the northern Gulf of Mexico. *Geophys. Res. Lett.* 38, L21404.
- Kolker, A.S., Cable, J.E., Johannesson, K.H., Allison, M.A., Inniss, L.V., 2013. Pathways and processes associated with the transport of groundwater in deltaic systems. *J. Hydrol.* 498, 319–334.
- Kostka, J.E., Luther, G.W., 1995. Seasonal cycling of Fe in salt marsh sediments. *Biogeochemistry* 29, 159–181.
- Krairapanond, N., Delaune, R.D., Patrick, W.H., 1992. Distribution of organic and reduced sulfur forms in marsh soils of coastal Louisiana. *Org. Geochem.* 18, 489–500.
- The Coastal Master Plan by the Coastal Protection and Restoration Authority. <http://coastal.la.gov/2017-coastal-master-plan/>.
- Li, Y., Gregory, S., 1974. Diffusion of ions in sea water and in deep-sea sediments. *Geochim. Cosmochim. Acta* 38, 703–714.
- Li, C.Y., White, J.R., Chen, C.S., Lin, H.C., Weeks, E., Galvan, K., Bargu, S., 2011. Summertime tidal flushing of Barataria Bay: transports of water and suspended sediments. *J. Geophys. Res. Oceans* 116.
- Li, L., Ren, J., Yan, Z., Liu, S., Wu, Y., Zhou, F., Liu, C., Zhang, J., 2014. Behavior of arsenic in the coastal area of the Changjiang (Yangtze River) Estuary: influences of water mass mixing, the spring bloom and hypoxia. *Cont. Shelf Res.* 80, 67–78.
- Lord, C.J., Church, T.M., 1983. The geochemistry of salt marshes—sedimentary iron diffusion, sulfate reduction, and pyritization. *Geochim. Cosmochim. Acta* 47, 1381–1391.
- Luther, G.W., Kostka, J.E., Church, T.M., Sulzberger, B., Stumm, W., 1992. Seasonal iron cycling in the salt marsh sedimentary environment—the importance of ligand complexes with Fe(II) and Fe(III) in the dissolution of Fe(III) minerals and pyrite, respectively. *Mar. Chem.* 40, 81–103.
- Luther, G.W., Shellenbarger, P.A., Brendel, P.J., 1996. Dissolved organic Fe(III) and Fe(II) complexes in salt marsh porewaters. *Geochim. Cosmochim. Acta* 60 (6), 951–960.
- Maher, D.T., Santos, I.R., Golsby-Smith, L., Gleeson, J., Eyre, B.D., 2013. Groundwater-derived dissolved inorganic and organic carbon exports from a mangrove tidal creek: the missing mangrove carbon sink? *Limnol. Oceanogr.* 58, 475–488.
- Makings, U., Santos, I.R., Maher, D.T., Golsby-Smith, L., Eyre, B.D., 2014. Importance of budgets for estimating the input of groundwater-derived nutrients to an eutrophic tidal river and estuary. *Estuar. Coast. Shelf Sci.* 143, 65–76.
- McBride, M.B., 1978. Transition metal bonding in humic acid: ESR study. *Soil Sci.* 126, 200–209.
- McBride, M.B., 1979. Mobility and reactions of VO₂⁺ on hydrated smectite surfaces. *Clay Clay Miner.* 27, 91–96.
- Menke, W., Menke, J., 2012. *Environmental Data Analysis with Matlab®*. Elsevier, Oxford, UK.
- Middelburg, J.J., Hoede, D., Vandersloot, H.A., Vanderweijden, C.H., Wijkstra, J., 1988. Arsenic, antimony and vanadium in the North Atlantic Ocean. *Geochim. Cosmochim. Acta* 52, 2871–2878.
- Miley, G.A., Kiene, R.P., 2004. Sulfate reduction and pore water chemistry in a gulf coast *Juncus roemerianus* (Needlerush) marsh. *Estuaries* 27, 472–481.

- Mohajerin, T.J., Helz, G.R., Johannesson, K.H., 2016. Tungsten-molybdenum fractionation in estuarine environments. *Geochim. Cosmochim. Acta* 177, 105–119.
- Moore, W.S., 1999. The subterranean estuary: a reaction zone of ground water and sea water. *Mar. Chem.* 65, 111–125.
- Moore, W.S., Blanton, J.O., Joye, S.B., 2006. Estimates of flushing times, submarine groundwater discharge, and nutrient fluxes to Okatee Estuary, South Carolina. *J. Geophys. Res.* 111.
- Morford, J.L., Emerson, S.R., Breckel, E.J., Kim, S.H., 2005. Diagenesis of oxyanions (V, U, Re, and Mo) in pore waters and sediments from a continental margin. *Geochim. Cosmochim. Acta* 69, 5021–5032.
- Morse, J.W., Millero, F.J., Cornwell, J.C., Rickard, D., 1987. The chemistry of hydrogen sulfide and iron sulfide systems in natural waters. *Earth-Sci. Rev.* 24, 1–42.
- Nickson, R., McArthur, J., Burgess, W., Ahmed, K.M., Ravenscroft, P., Rahmann, M., 1998. Arsenic poisoning of Bangladesh groundwater. *Nature* 395 (6700), 338.
- Nordstrom, D.K., Archer, D.G., 2003. Arsenic thermodynamic data and environmental geochemistry. In: Welch, A.H., Stollenwerk, K.G. (Eds.), *Arsenic in Groundwater: Geochemistry and Occurrence*. Kluwer Academic Press, Boston, pp. 1–25.
- Nordstrom, D.K., Majzlan, J., Königsberger, E., 2014. Thermodynamic properties for arsenic minerals and aqueous species. *Rev. Mineral. Geochem.* 79 (1), 217–255.
- O'Connor, M.T., Moffett, K.B., 2015. Groundwater dynamics and surface water-groundwater interactions in a prograding delta island, Louisiana, USA. *J. Hydrol.* 524, 15–29.
- O'Connor, A.E., Lueck, J.L., McIntosh, H., Beck, A.J., 2015. Geochemistry of redox-sensitive trace elements in a shallow subterranean estuary. *Mar. Chem.* 172, 70–81.
- O'Day, P.A., Vlassopoulos, D., Root, R., Rivera, N., 2004. The influence of sulfur and iron on dissolved arsenic concentrations in the shallow subsurface under changing redox conditions. *Proc. Natl. Acad. Sci. U. S. A.* 101, 13,703–13,708.
- Olesik, 2014. Inductively coupled plasma mass spectrometers. In: *Treatise on Geochemistry*, second ed. 15. pp. 209–336.
- Pakhomova, S.V., Hall, P.O.J., Kononets, M.Y., Rozanov, A.G., Tengberg, A., Vershinin, A.V., 2007. Fluxes of iron and manganese across the sediment-water interface under various redox conditions. *Mar. Chem.* 107, 319–331.
- Park, D., 2002. Hydrodynamics and Freshwater Diversion Within Barataria Basin, Ph.D. Dissertation. La. State Univ., Baton Rouge (112 pp).
- Paytan, A., Shellenbarger, G.G., Street, J.H., Gonnesa, M.E., Davis, K., Young, M.B., Moore, W.S., 2006. Submarine groundwater discharge: an important source of inorganic nitrogen to coral reef ecosystems. *Limnol. Oceanogr.* 51 (1), 343–348.
- Peacock, C.L., Sherman, D.M., 2004. Vanadium(V) adsorption onto goethite (alpha-FeOOH) at pH 1.5 to 12: a surface complexation model based on ab initio molecular geometries and EXAFS spectroscopy. *Geochim. Cosmochim. Acta* 68, 1723–1733.
- Planer-Friedrich, B., London, J., McCleskey, R.B., Nordstrom, D.K., Wallschläger, D., 2007. Thioarsenates in geothermal waters of Yellowstone National Park: determination, preservation, and geochemical importance. *Environ. Sci. Technol.* 41, 5245–5251.
- Planer-Friedrich, G., Franke, D., Merkel, B., Wallschläger, D., 2008. Acute toxicity of thioarsenates to *Vibrio fischeri*. *Environ. Toxicol. Chem.* 27 (10), 2027–2035.
- Pourret, O., Dia, A., Gruau, G., Davranche, M., Bouhnik-Le Coz, M., 2012. Assessment of vanadium distribution in shallow groundwaters. *Chem. Geol.* 294–295, 89–102.
- Reed, D.J., 1995. The response of coastal marshes to sea-level rise: survival or submergence. *Earth Surf. Process. Landf.* 20, 39–48.
- Ren, J.L., Zhang, J., Li, D.D., Cheng, Y., Liu, S.M., 2010. Behavior of dissolved inorganic arsenic in the Yellow Sea and East China Sea. *Deep-Sea Res. II Top. Stud. Oceanogr.* 57, 1035–1046.
- Rickard, D., 2006. The solubility of FeS. *Geochim. Cosmochim. Acta* 70 (23), 5779–5789.
- Rimmer, S.M., 2004. Geochemical paleoredox indicators in Devonian-Mississippian black shales, central Appalachian basin (USA). *Chem. Geol.* 206, 373–391.
- Rochette, E.A., Bostick, B., Li, G., Fendorf, S., 2000. Kinetics of arsenate reduction by dissolved sulfide. *Environ. Sci. Technol.* 34, 4714–4720.
- Rose, A.L., Waite, T.D., 2003. Kinetics of iron complexation by dissolved natural organic matter in coastal waters. *Mar. Chem.* 84 (1), 85–103.
- Sanders, C.J., Santos, I.R., Maher, D.T., Sadat-Noori, M., Schnetger, B., Brumsack, H.J., 2015. Dissolved iron exports from an estuary surrounded by coastal wetlands: can small estuaries be a significant source of Fe to the ocean? *Mar. Chem.* 176, 75–82.
- Sankar, M.S., Vega, M.A., Defoe, P.P., Kibria, M.G., Ford, S., Telfeyan, K., Neal, A., Mohajerin, T.J., Hettiarachchi, G.M., Barua, S., Hobson, C., Johannesson, K.H., Datta, S., 2014. Elevated arsenic and manganese in groundwaters of Murshidabad, West Bengal, India. *Sci. Total Environ.* 488–489, 570–579.
- Santos, I.R., Burnett, W.C., Misra, S., Suryaputra, I.G.N.A., Chanton, J.P., Dittmar, T., Peterson, R.N., Swarzenski, P.W., 2011. Uranium and barium cycling in a salt wedge subterranean estuary: the influence of tidal pumping. *Chem. Geol.* 287.
- Santos-Echeandía, J., Prego, R., Cobelo-García, A., Millward, G.E., 2009. Porewater geochemistry in a Galician Ria (NW Iberian Peninsula): implications for benthic fluxes of dissolved trace elements (Co, Cu, Ni, Pb, V, Zn). *Mar. Chem.* 117, 77–87.
- Santos-Echeandía, J., Vale, C., Caetano, M., Pereira, P., Prego, R., 2010. Effects of tidal flooding on metal distribution in pore waters of marsh sediments and its transport to water column (Tagus estuary, Portugal). *Mar. Environ. Res.* 70, 358–367.
- Schoonen, M.A.A., Barnes, H.L., 1991a. Reactions forming pyrite and marcasite from solution: I. Nucleation of FeS₂ below 100 °C. *Geochim. Cosmochim. Acta* 55 (6), 1495–1504.
- Schoonen, M.A.A., Barnes, H.L., 1991b. Reactions forming pyrite and marcasite from solutions: II. FeS precursors below 100 °C. *Geochim. Cosmochim. Acta* 55, 1505–1514.
- Shaw, T.J., Gieskes, J.M., Jahnke, R.A., 1990. Early diagenesis in differing depositional environments—the response of transition metals in pore water. *Geochim. Cosmochim. Acta* 54, 1233–1246.
- Shen, Z., Dawers, N.H., Törnqvist, T., Gasparini, N.M., Hijma, M.P., Mauz, B., 2016. Mechanisms of late Quaternary fault throw-rate variability along the north central Gulf of Mexico coast: implications for coastal subsidence. *Basin Res.* 1–4.
- Shiller, A.M., 1997. Dissolved trace elements in the MSR: seasonal, interannual, and decadal variability. *Geochim. Cosmochim. Acta* 61, 4321–4330.
- Shiller, A.M., Mao, L.J., 1999. Dissolved vanadium on the Louisiana Shelf: effect of oxygen depletion. *Cont. Shelf Res.* 19, 1007–1020.
- Shiller, A.M., Mao, L.J., 2000. Dissolved vanadium in rivers: effects of silicate weathering. *Chem. Geol.* 165, 13–22.
- Slomp, C.P., Van Cappellen, P., 2004. Nutrient inputs to the coastal ocean through submarine groundwater discharge: controls and potential impact. *J. Hydrol.* 295, 64–86.
- Smedley, P.L., Kinniburgh, D.G., 2002. A review of the source, behavior and distribution of arsenic in natural waters. *Appl. Geochem.* 17 (5), 517–568.
- Smith, C.G., Cable, J.E., Martin, J.B., Roy, M., 2008. Evaluating the source and seasonality of submarine groundwater discharge using a radon-222 pore water transport model. *Earth Planet. Sci. Lett.* 273 (3), 312–322.
- Stauder, S., Raue, B., Sacher, F., 2005. Thioarsenates in sulfidic waters. *Environ. Sci. Technol.* 39, 5933–5939.
- Steinmann, P., Shotyk, W., 1997. Chemical Composition, pH, and Redox State of Sulfur and Iron in Complete Vertical Profiles From Two *Sphagnum* Peat Bogs, Jura Mountains, Switzerland. 61(6). pp. 1143–1163.
- Stumpp, C., Ekdal, A., Gonenc, I.E., Maloszewski, P., 2014. Hydrological dynamics of water sources in a Mediterranean lagoon. *Hydrol. Earth Syst. Sci.* 18, 4825–4837.
- Sullivan, K.A., Aller, A.C., 1996. Diagenetic cycling of arsenic in Amazon shelf sediments. *Geochim. Cosmochim. Acta* 60 (9), 1465–1477.
- Sundby, B., Vale, C., Caetano, M., Luther, G.W., 2003. Redox chemistry in the root zone of a salt marsh sediment in the Tagus Estuary, Portugal. *Aquat. Geochem.* 9, 257–271.
- Swarzenski, P.W., Baskaran, M., 2007. Uranium distribution in the coastal waters and pore waters of Tampa Bay, Florida. *Mar. Chem.* 104, 43–57.
- Telfeyan, K., Johannesson, K.H., Mohajerin, T.J., Palmore, C.D., 2015. Vanadium geochemistry in contrasting aquifers of the United States: Carrizo Sand (Texas) and Oasis Valley (Nevada) aquifers. *Chem. Geol.* 410, 63–78.
- Trefry, J.H., Metz, S., 1989. Role of hydrothermal precipitates in the geochemical cycling of vanadium. *Nature* 342, 531–533.
- Tribouillat, N., Algeo, T.J., Lyons, T., Riboulleau, A., 2006. Trace metals as paleoredox and paleoproductivity proxies: an update. *Chem. Geol.* 232, 12–32.
- Turetta, C., Capodaglio, G., Cairns, W., Rabar, S., Cescon, P., 2005. Benthic fluxes of trace metals in the lagoon of Venice. *Microchem. J.* 79, 149–158.
- Van der Weijden, C.H., Middelburg, J.J., Delange, G.J., Vandersloot, H.A., Hoede, D., Woitiez, J.R.W., 1990. Profiles of the redox sensitive trace elements As, Sb, V, Mo and U in the Tyro and Bannock Basin (Eastern Mediterranean). *Mar. Chem.* 31, 171–186.
- Wallschläger, D., Stadey, C.J., 2007. Determination of (oxy)thioarsenates in sulfidic waters. *Anal. Chem.* 79, 3873–3880.
- Wanty, R.B., Goldhaber, M.B., 1992. Thermodynamics and kinetics of reactions involving vanadium in natural systems—accumulation of vanadium in sedimentary rocks. *Geochim. Cosmochim. Acta* 56, 1471–1483.
- Warnken, K.W., Gill, G.A., Griffin, L.L., Santschi, P.H., 2001. Sediment-water exchange of Mn, Fe, Ni and Zn in Galveston Bay, Texas. *Mar. Chem.* 73, 215–231.
- Webster, J.G., 1990. The solubility of As₂S₃ and speciation of As in dilute and sulphide-bearing fluids at 25 and 90 °C. *Geochim. Cosmochim. Acta* 54, 1009–1017.
- Wehrli, B., Stumm, W., 1989. Vanadyl in natural waters: adsorption and hydrolysis promote oxygenation. *Geochim. Cosmochim. Acta* 53, 69–77.
- Wilkin, R.T., Ford, R.G., 2006. Arsenic solid-phase partitioning in reducing sediments of a contaminated wetland. *Chem. Geol.* 228, 156–174.
- Wilson, C.A., Allison, M.A., 2008. An equilibrium profile model for retreating marsh shorelines in southeast Louisiana. *Estuar. Coast. Shelf Sci.* 80 (4), 483–494.
- Windom, H., Niencheski, F., 2003. Biogeochemical processes in a freshwater-seawater mixing zone in permeable sediments along the coast of Southern Brazil. *Mar. Chem.* 83, 121–130.
- Windom, H.L., Moore, W.S., Niencheski, L.F.H., Jahrike, R.A., 2006. Submarine groundwater discharge: a large, previously unrecognized source of dissolved iron to the South Atlantic Ocean. *Mar. Chem.* 102, 252–266.
- Wolthers, M., Charlet, L., van der Weijden, C., van der Linde, P.R., Rickard, D., 2005. Arsenic mobility in the ambient sulfidic environment: sorption of arsenic(V) and arsenic(III) onto disordered mackinawite. *Geochim. Cosmochim. Acta* 69 (14), 3483–3492.
- Wolthers, M., Butler, I.B., Rickard, D., 2007. Influence of arsenic on iron sulfide transformations. *Chem. Geol.* 236, 217–227.
- Wright, M.T., Belitz, K., 2010. Factors controlling the regional distribution of vanadium in groundwater. *Ground Water* 48 (4), 515–525.
- Wright, M.T., Stollenwerk, K.G., Belitz, K., 2014. Assessing the solubility controls on vanadium in groundwater, northeastern San Joaquin Valley, CA. *Appl. Geochem.* 48, 41–52.
- Wurl, O., Shelley, R.U., Landing, W.M., Cutter, G.A., 2015. Biogeochemistry of dissolved arsenic in the temperate to tropical North Atlantic Ocean. *Deep-Sea Res. II Top. Stud. Oceanogr.* 116, 240–250.
- Yang, N.F., Welch, K.A., Mohajerin, T.J., Telfeyan, K., Chevis, D.A., Grimm, D.A., Lyons, W.B., White, C.D., Johannesson, K.H., 2015. Comparison of arsenic and molybdenum geochemistry in meromictic lakes of the McMurdo Dry Valleys, Antarctica: implications for oxyanion-forming trace element behavior in permanently stratified lakes. *Chem. Geol.* 404, 110–125.
- Yang, N., Shen, Z., Datta, S., Johannesson, K.H., 2016. High arsenic (As) concentrations in the shallow groundwaters of southern Louisiana: evidence of microbial controls on As mobilization from sediments. *J. Hydrol. Region. Stud.* 5, 100–113.
- Zhu, C., Anderson, G., 2002. *Environmental Applications of Geochemical Modeling*. Cambridge University Press, Cambridge, UK (284 p).